Check for updates

annalen der physik
www.ann-phys.org

Probabilistic Discrete-Time Models for Spreading Processes in Complex Networks: A Review

*Clara Granell, Sergio Gómez, Jesús Gómez-Gardeñes, and Alex Arenas**

Research into network dynamics of spreading processes typically employs both discrete and continuous time methodologies. Although each approach offers distinct insights, integrating them can be challenging, particularly when maintaining coherence across different time scales. This review focuses on the Microscopic Markov Chain Approach (MMCA), a probabilistic f ramework originally designed for epidemic modeling. MMCA uses discrete dynamics to compute the probabilities of individuals transitioning between epidemiological states. By treating each time step—usually a day—as a discrete event, the approach captures multiple concurrent changes within this time frame. The approach allows to estimate the likelihood of individuals or populations being in specific states, which correspond to distinct epidemiological compartments. This review synthesizes key findings from the application of this approach, providing a comprehensive overview of its utility in understanding epidemic spread.

1. Introduction

The interplay between network structures and spreading dynamics has played a pivotal role in advancing the field of network science. On one hand, understanding epidemic spreading within networks has been crucial to capture the influence that complex interaction patterns have on the functioning of complex systems, as highlighted by seminal works in the field such as ref. [1–3] and the references therein. On the other hand, dynamical network models have been instrumental to provide formal frameworks to simulate and predict the spread of diseases.[4] In contrast to traditional approaches, which often oversimplify these interactions, network epidemic models capture the nuances of spreading processes in general which, in the case of disease transmission, facilitates the exploration of intervention strategies.

Compartmental models, dividing populations into distinct epidemiological states, form the foundation of mathematical epidemiological models to conceptualize disease evolution. These models underpin more complex frameworks. Epidemic models vary widely, being either deterministic or stochastic,[5] to reflect transmission predictability or randomness. They differ in assumptions of homogeneous versus heterogeneous mixing,[6] spatial[7] versus individual-level networks, and static versus dynamic networks.[8] Furthermore, models can focus on single or multiple dynamics, including co-evolving diseases[9] or coupled social and epidemiological processes.[10]

A key aspect of mathematical modeling in epidemics, and generally speaking in spreading processes, is choosing between continuous or discrete time approaches to describe spread. Initially, epidemiological models predominantly used differential equations to represent how the proportion of individuals in each compartment changes over time. However, discrete models emerged,[11] challenging this approach by emphasizing that epidemic processes often unfold in discrete time intervals. This perspective is supported by the reality that data collection in real-world scenarios typically occurs on a daily basis, at best.

In this review, we examine the Microscopic Markov Chain Approach (MMCA),[12] a discrete-time probabilistic framework for modeling the dynamics of spreading processes, such as epidemics, on complex networks. MMCA is based on the principles of Markov chains, which are mathematical systems undergoing transitions from one state to another within a state space in a memoryless manner; this implies that the next state depends solely on the current state, irrespective of the sequence of events that preceded it. Initially proposed for epidemic modeling, the applicability of MMCA extends to various other spreading phenomena, leveraging the same formalism.

This review systematically discusses the Microscopic Markov Chain Approach (MMCA) for modeling spreading processes

C. Granell, S. Gómez, A. Arenas
Departament d'Enginyeria Informàtica i Matemàtiques
Universitat Rovira i Virgili
Tarragona 43007, Spain
E-mail: alexandre.arenas@urv.cat

J. Gómez-Gardeñes
Department of Condensed Matter Physics
University of Zaragoza
Zaragoza 50010, Spain

J. Gómez-Gardeñes
GOTHAM Lab–Institute for Biocomputation and Physics of Complex Systems (BIFI)
University of Zaragoza
Zaragoza 50018, Spain

The ORCID identification number(s) for the author(s) of this article can be found under https://doi.org/10.1002/andp.202400078

© 2024 The Author(s). Annalen der Physik published by Wiley-VCH GmbH. This is an open access article under the terms of the Creative Commons Attribution-NonCommercial-NoDerivs License, which permits use and distribution in any medium, provided the original work is properly cited, the use is non-commercial and no modifications or adaptations are made.

DOI: 10.1002/andp.202400078

on networks in discrete time. Section 2 revisits the fundamentals of epidemic spreading in networks. Subsequently, Section 3 elucidates the principal differences between discrete-time and continuous-time descriptions of epidemic modeling in networks. Section 4 is dedicated to detailing the MMCA approach, which describes epidemics at the individual node level, at the link level, accounts for beyond pairwise interactions, and incorporates time-dependent network aspects. In Section 5, we explore applications involving different layers of interactions, specifically within multilayer networks. Section 6 demonstrates the framework's applicability to tracking real-world epidemics. Finally, we present conclusions and future perspectives on the approach.

2. Epidemics Spreading in Networks: The Basics

Complex networks are interconnected systems characterized by non-trivial topological features' patterns of connection between elements that are neither purely regular nor completely random. These networks are distinguished by properties such as scale-free degree distributions, where some nodes act as highly connected hubs; small-world phenomena, where paths between any two nodes are surprisingly short; and clustering, indicating a tendency for nodes to form tightly-knit groups. Complex networks are ubiquitous in nature and society, underpinning the structure and dynamics of systems ranging from biological entities and ecosystems to social networks, technological infrastructures, and beyond.

The study of complex networks[13] has advanced our understanding of contagion dynamics. Particularly important is the ubiquity of the so-called Scale-free (SF) networks in social interactions, characterized by a degree distribution that follows a power law, $P(k) \sim k^{-\gamma}$, where k represents the number of connections an individual has. A key mathematical framework to understand epidemic outbreaks in SF networks is the so-called Heterogeneous Mean Field (HMF) approach,[14–18] which aggregates vertices within degree classes, assuming homogeneity in dynamical properties within each class and neglecting fluctuations.

In the simplest epidemic models consisting on just two compartments, susceptible (S) and infectious (I), the spreading of a disease on a network can be conceptualized as the evolution of a set of variables $\{\rho_k(t)\}$ each capturing the relative density of infected nodes with given connectivity k at time t. Once these variables are defined we can write the HMF equations that govern their evolution under a certain set of transition rules. In the case of a SIS epidemic two transitions are at work: the transmission $S \to I$ and the recovery $I \to S$, each having transition rates β and μ respectively. Thus, the dynamical mean–field (MF) reaction rate equations can be expressed as:

$$\frac{d}{dt}\rho_k(t) = -\mu\rho_k(t) + \beta k(1-\rho_k(t))\Theta(\beta) \tag{1}$$

where $\Theta(\beta)$ is the probability that any given link points to an infected node. The term $-\mu\rho_k(t)$ represents the annihilation term, i.e., those infected nodes that recover, and correspondingly, the term $\beta k(1-\rho_k(t))\Theta(\beta)$ represents the creation term, accounting for the probability that a node with k links is healthy and becomes infected through a connected node.

The mean-field character of this equation arises from neglecting density correlations among different nodes, albeit relaxing the homogeneity assumption on node connectivity typically applied in regular networks. By setting $\frac{d}{dt}\rho_k(t) = 0$, the stationary densities are found:

$$\rho_k = \frac{\beta k \Theta(\beta)}{\mu + \beta k \Theta(\beta)} \tag{2}$$

indicating that higher node connectivity increases the probability of infection. This inhomogeneity is crucial for the self-consistent calculation of $\Theta(\beta)$. The probability that a link points to a node with s links is proportional to $sP(s)$, implying that a randomly chosen link is more likely to connect to a high-connectivity node:

$$\Theta(\beta) = \frac{1}{\langle k \rangle}\sum_k kP(k)\rho_k \tag{3}$$

Given that $\Theta(\beta)$ is a function of ρ_k, a consistency equation can be obtained, enabling the determination of the solution, $\{\rho_k\}$ of Equation (2). The resulting values are encapsulated in the order parameter, which expresses the average density of infected nodes in the system, which can be calculated as

$$\rho = \sum_k P(k)\rho_k \tag{4}$$

This approach effectively describes the critical properties of epidemic spreading in heterogeneous networks, especially in scale-free (SF) networks. A simple analysis yields $\rho \approx 2e^{-\mu/\beta}$, aligning with numerical findings and highlighting the absence of an epidemic threshold (β_c) or critical point in the model, i.e., $\beta_c \approx 0$ (see **Figure 1**). However, capturing the temporal evolution of epidemics is challenging with this method, as it neglects the specific routes of infection. The approach does not consider a particular realization of the network but concentrates solely on the degree distribution $P(k)$, making it challenging to explore the detailed network structure beyond this statistical descriptor. While incorporating degree correlations[19] has improved the mathematical analysis of the critical point, it still falls short of capturing the time evolution within a specific network topology.

3. Discrete-Time and Continuous-Time Epidemic Models in Networks

The analysis of epidemic-spreading models in networks has some of the same difficulties that are found for well-mixed populations (equivalent to complete graphs). These difficulties are intrinsic to the discrete-time or continuous-time formulation of the governing equations, and the methods used to solve each of them. Continuous approximations have been more popular in epidemic modeling because of their mathematical tractability, and the avoidance of chaotic behaviors that can arise in their discrete counterparts.[11] For the sake of clarity, we henceforth fix our attention on the study of a family of SIS models. In a SIS model, individuals that are cured do not develop permanent immunity but are immediately susceptible to the disease again. In well-mixed populations, the differential equations governing the

© 2024 The Author(s). Annalen der Physik published by Wiley-VCH GmbH

15213889, 0, Downloaded from https://onlinelibrary.wiley.com/doi/10.1002/andp.202400078 by Universidad De Zaragoza, Wiley Online Library on [12/09/2024]. See the Terms and Conditions (https://onlinelibrary.wiley.com/terms-and-conditions) on Wiley Online Library for rules of use; OA articles are governed by the applicable Creative Commons License

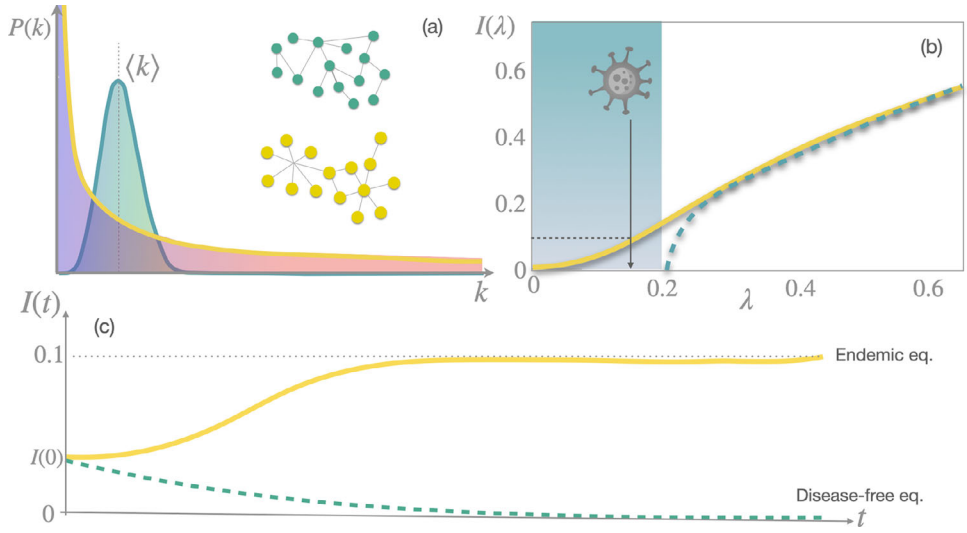

Figure 1. Absence of epidemic threshold in scale-free networks. a) Degree distributions of an Erdős–Rényi graph (blue) and a scale-free network (yellow) with identical mean degree $\langle k \rangle$. The large variance of the scale-free network is highlighted by the presence of large degree nodes (the hubs). In panel (b) we show the expected epidemic diagram $I(\lambda)$ for the SIS compartmental model in ER and SF graphs. Panel (c) shows the effect of introducing a pathogen with an infectivity β in the range shown in panel (b). While the introduction of the pathogen in the ER graph leads to the disease-free equilibrium ($I = 0$), the same pathogen yields an endemic equilibrium in SF networks.

number of susceptible (S) and infected (I) individuals are

$$\frac{dS}{dt} = -\tilde{\beta} S \frac{I}{N} + \tilde{\mu} I$$
$$\frac{dI}{dt} = \tilde{\beta} S \frac{I}{N} - \tilde{\mu} I \tag{5}$$

where $N = S(t) + I(t)$ is the (constant) size of the population. The term I/N accounts for the probability of contacting an infected individual in a well-mixed population of size N, $\tilde{\beta}$ is the infectivity rate (probability per unit time) for each contact, and $\tilde{\mu}$ is the rate at which one infected individual recovers. Their corresponding difference equations are

$$S(t + \Delta t) = S(t)\left(1 - \tilde{\beta}\Delta t \frac{I(t)}{N}\right) + \tilde{\mu}\Delta t I(t)$$
$$I(t + \Delta t) = I(t)\left[1 - \tilde{\mu}\Delta t + \tilde{\beta}\Delta t \frac{I(t)}{N} S(t)\right] \tag{6}$$

or equivalently

$$I(t + \Delta t) = I(t) - \tilde{\mu}\Delta t I(t) + \tilde{\beta}\Delta t \frac{I(t)}{N}[N - I(t)] \tag{7}$$

Defining $\rho(t) = I(t)/N$ as the fraction of infected individuals in the population, Equation (7) is written as

$$\rho(t + \Delta t) = \rho(t) - \tilde{\mu}\Delta t\, \rho(t) + \tilde{\beta}\Delta t\, \rho(t)[1 - \rho(t)] \tag{8}$$

Note that while the system of Equation (5) always converges to a solution,[11,20] Equation (8) can be mapped to a logistic function when the reproductive ratio $\mathcal{R} = \tilde{\beta}/\tilde{\mu} > 1$, thus giving rise to basic periodicity, bifurcations and chaotic behavior depending on the parameters.[11] Although both descriptions are equivalent in the limit $\Delta t \to 0$, differences arise when considering a finite Δt.

Particularly interesting is what happens when considering a numerical scheme iterating Equation (8). In many cases Δt is usually assimilated to the stochastic simulation time unit and set to 1. Consequently, the numerical differences with the continuous case are substantial. It is also important to distinguish between rates and probabilities, $\tilde{\beta}\Delta t = \beta$ is a probability, and the same holds for $\tilde{\mu}\Delta t = \mu$. Again, by setting $\Delta t = 1$, one can mix up rate and probabilities because both will have the same values, even though their units are different.

The mapping of the above SIS equations to the case of heterogeneous networks is not straightforward and has its critical step in the redefinition of the probability of contacts. In a network, the number of contacts is restricted to a fixed neighborhood, then each individual (node) can potentially contact only its neighbors. In the seminal work by Pastor–Satorras and Vespignani,[21] these authors proposed the direct use of Equation (8) for classes of nodes based on their degree k. This is the root of the HMF approach in complex networks and the hypothesis of homogeneity is here postulated at the level of classes of nodes. The rationale behind this assumption is that the dynamical behavior of any two nodes with the same degree k will be essentially the same. Then, a system of equations for each class k is written as

$$\rho_k(t + \Delta t) = \rho_k(t) - \tilde{\mu}\Delta t\, \rho_k(t) + \tilde{\beta}\Delta t\, \Theta_k(t)[1 - \rho_k(t)] \tag{9}$$

where now $\rho_k(t)$ stands for the fraction of infected individuals of degree k, and the probability of contacting an infected node is encoded in the new function $\Theta_k(t)$. For the general case of correlated networks, the function $\Theta_k(t)$ takes the form

$$\Theta_k(t) = \sum_{k'} P(k'|k)\rho_{k'} \tag{10}$$

where $P(k'|k)$ is the probability that a node of degree k connects to a node of degree k'. Equation (9) is used to find the stationary

© 2024 The Author(s). Annalen der Physik published by Wiley-VCH GmbH

15213889, 0, Downloaded from https://onlinelibrary.wiley.com/doi/10.1002/andp.202400078 by Universidad De Zaragoza, Wiley Online Library on [12/09/2024]. See the Terms and Conditions (https://onlinelibrary.wiley.com/terms-and-conditions) on Wiley Online Library for rules of use; OA articles are governed by the applicable Creative Commons License

value of the incidence for given values of β and μ. Indeed, for the stationary state, it is true that the only dependence to take into account is the ratio $\lambda = \beta/\mu$ because the equations can be rescaled without modifying their solutions. However, this is not anymore the case during the transient. The critical value λ_c for the epidemic threshold was found in ref. [22] to be

$$\lambda_c = \frac{1}{\Lambda_{max}(C)} \tag{11}$$

being $\Lambda_{max}(C)$ the largest eigenvalue of the connectivity matrix of classes of nodes C, whose components are given by $C_{kk'} = kP(k'|k)$, i.e., the expected number of links from a node of degree k to nodes of degree k'. Recently, several authors have conducted extensive research to uncover the differences in accuracy between continuous and discrete models for the SIS dynamics on networks.[23] This analysis includes examining the epidemic threshold and the localization of epidemic prevalence near the transition. The findings indicate that discrete-time approaches exhibit dependence on the size of the time-step, whereas the differences between discrete and continuous models diminish as the time-step approaches zero. It is important to highlight that this result is applicable to the discretization of continuous equations but may not extend to discrete models developed ab initio. In such models, specific aspects, such as the possibility of recovery and reinfection within the same time step, can be explicitly considered or omitted. Note that, even if discrete-time models can recover the continuous-time dynamics in the limit of vanishing time-steps, there are implicit differences that can yield a few distinct results. For instance, in the most standard discrete-time models, a node can be infected or recovered only once per time step whereas, in the same time span, a continuous-time dynamic allows several changes of state. These nuances can significantly influence the comparison between both modeling approaches.

4. Microscopic Markov Chain Approach to Epidemic Spreading

The approach to describing epidemic spreading using HMF in networks has been very successful in ascertaining the critical properties of the dynamics. However, it has been noted that these methods are unable to track the specific evolution of an epidemic outbreak, as such evolution is entirely dependent on the particular structure of a network.

To describe epidemic spreading at the microscopic level (individual nodes), several researchers have identified that the state of the system in the SIS model can be precisely defined by a set of Bernoulli random variables $x_i(t) \in \{0, 1\}$, where $x_i(t) = 0$ represents a healthy, susceptible node, and $x_i(t) = 1$ denotes an infected node. The expectation of this variable, $\bar{x}_i(t) = \rho_i^I(t)$, represents the probability of node i being infected. It is feasible to construct a 2^N Markov chain [24–26], accurately delineating the time evolution of the SIS model. This enables the formulation of precise equations for the expectation of infection for each node i in the SIS model:

$$\frac{d\rho_i^I(t)}{dt} = -\mu\rho_i^I(t) + \beta\sum_{j=1}^{N} a_{ij}\left[\rho_i^I(t) - \langle x_i(t)x_j(t)\rangle\right] \tag{12}$$

where $\langle\cdots\rangle$ denotes the expected value. However, this equation requires knowledge of the history of individual states or the joint probability distribution of all pairs of nodes i, j. A workaround is found in the mean-field approximation, assuming independence of the states of nodes, $\langle x_i x_j\rangle = \rho_i^I\rho_j^I$, the equation simplifies[27,28]:

$$\frac{d\rho_i^I(t)}{dt} = -\mu\rho_i^I(t) + \beta\left[1 - \rho_i^I(t)\right]\sum_{j=1}^{N} a_{ij}\rho_j^I(t) \tag{13}$$

4.1. Microscopic Markov Chain Approach for Individual Nodes in Networks

The Microscopic Markov Chain Approach (MMCA) introduced in ref. [12] offers a compatible yet distinct perspective. It describes the discrete-time nature of epidemic data evolution from scratch and does not correspond to a discretization of previous continuous models. Simply put, the MMCA cannot be derived from a discretization of continuous equations; rather, the continuous equations can be derived from the MMCA description.

Let us describe the basics of the MMCA. Consider a network of N nodes represented by an $N \times N$ adjacency matrix $\mathbf{A}$. In cases where the network is weighted, $\{\omega_{ij}\}$ denote the connection weights, with $w_i = \sum_j \omega_{ij}$ representing node i's total strength. This framework, incorporating a discrete two-state (S and I) contact-based process, precisely maps the dynamics of infection spread across the network. At each timestep, an infected node i attempts c_i times to transmit the disease to its neighbors with probability β, forming a Markov chain where infection probability depends solely on the previous timestep. After a transient period, the system reaches a stationary state where ρ, the average density of infected individuals, indicates disease prevalence.

The probability that a given node i is in contact with a node j is denoted as r_{ij}, and captured by a matrix $\mathbf{R}$, with entries indicating the transmission probabilities across network links. If nodes i and j are unconnected, then $r_{ij} = 0$. Note that this matrix corresponds to the usage of matrix $\mathbf{A}$ in the epidemic process, i.e., the effective use of the links of the graph to transmit the epidemics at each time step t. The recovery rate μ indicates the rate at which infected nodes revert to susceptibility, and $p_i(t)$ is the probability of node i being infected at time t. The evolution of node i's infection probability is given by:

$$p_i(t+1) = (1 - q_i(t))(1 - p_i(t)) + (1 - \mu)p_i(t) + \mu(1 - q_i(t))p_i(t) \tag{14}$$

where $q_i(t)$ represents the probability of node i not being infected by any neighbor:

$$q_i(t) = \prod_{j=1}^{N}(1 - \beta r_{ji}p_j(t)) \tag{15}$$

The first term on the right-hand side of Equation (14) represents the probability that node i is susceptible, $(1 - p_i(t))$, and becomes infected, $(1 - q_i(t))$, by at least one neighbor. The second term corresponds to the probability that node i is already infected at time t and does not recover. Finally, the last term accounts for the probability that an infected node recovers, $\mu p_i(t)$, but is subsequently re-infected by at least one neighbor, $(1 - q_i(t))$.

© 2024 The Author(s). Annalen der Physik published by Wiley-VCH GmbH

15213889, 0, Downloaded from https://onlinelibrary.wiley.com/doi/10.1002/andp.202400078 by Universidad De Zaragoza, Wiley Online Library on [12/09/2024]. See the Terms and Conditions (https://onlinelibrary.wiley.com/terms-and-conditions) on Wiley Online Library for rules of use; OA articles are governed by the applicable Creative Commons License

This model allows for recovery and infection to occur on the same timescale, enabling re-infection within discrete time windows. Two different situations of interest are considered: 1) without one-step reinfections (WOR), and 2) with one-step reinfections (WIR). The first case implies that the time scales for the infection and cure are well separated, whereas the latter assumes that the same time scale holds for infection and cure and therefore a just recovered individual might catch the disease again within the same time step t. Note that this differentiation between both simulation proposals (WIR and WOR) do not change the aim of the infection dynamics, which in both cases is compatible with the SIS class of models, not with the SIR class.

The respective equations are:

WOR:

$$p_i(t+1) = [1 - p_i(t)][1 - q_i(t)] + (1 - \mu)p_i(t) \tag{16}$$

WIR:

$$p_i(t+1) = [1 - q_i(t)] + (1 - \mu)p_i(t)q_i(t) \tag{17}$$

where the probability $q_i(t)$ of node i not being infected by any neighbor is

$$q_i(t) = \prod_{j=1}^{N}[1 - \beta r_{ji}p_j(t)] \tag{18}$$

Keeping in mind the separation of the two processes, namely, contacting a node and transmitting the infection, already presented in Equation (6) for the well-mixed case, the explanation of these equations is straightforward. The terms in the r.h.s. of Equation (16) account respectively for the probability that a susceptible node $[1 - p_i(t)]$ is infected by at least one neighbor $[1 - q_i(t)]$, and an infected node does not recover $[(1 - \mu)p_i(t)]$. Equation (17) adds, after some algebra, a term that accounts for the probability that an infected node recovers $[\mu p_i(t)]$ but gets infected again by a neighbor $[1 - q_i(t)]$ in the same time step. Finally, in Equation (18), we represent the probabilities that infected nodes $[p_j(t)]$ contact node i, and that these contacts lead to new infections, which occur with probability β.

The MMCA approach generalizes previous models by accommodating the possibility of re-infections, which were not considered in earlier formulations. The formulation so far relies on the assumption that the probabilities of being infected p_i are independent random variables. This hypothesis turns out to be valid in the vast majority of complex networks because the inherent topological disorder makes dynamical correlations not persistent. The dynamical system, represented by Equations (14) and (15), corresponds to a family of possible models, parameterized by the explicit form of the contact probabilities r_{ij}. Without loss of generality, it is instructive to think of these probabilities as the transition probabilities of random walkers on the network. The general case is represented by c_i random walkers leaving node i at each time step:

$$r_{ij} = 1 - \left(1 - \frac{\omega_{ij}}{w_i}\right)^{c_i} \tag{19}$$

The Contact Process (CP) corresponds to a model dynamics of one contact per unit time, $c_i = 1$, for all i in Equation (19), thus $r_{ij} = \frac{\omega_{ij}}{w_i}$. In the Reaction Process (RP), all neighbors are contacted, which corresponds, in this description, to setting the limit $c_i \to \infty$, for all i, resulting in $r_{ij} = a_{ij}$ regardless of whether the network is weighted or not. Other prescriptions for c_i conform to the spectrum of models that can be obtained using this unified framework. The phase diagram of every model is simply obtained by solving the system formed by Equations (17) or (16) for $i = 1, \dots, N$ at the stationary state:

WOR:

$$p_i = (1 - p_i)(1 - q_i) + (1 - \mu)p_i \tag{20}$$

WIR:

$$p_i = (1 - q_i) + (1 - \mu)p_i q_i \tag{21}$$

These equations always have the trivial disease-free solution $p_i = 0$, for all $i = 1, \dots, N$. Other non-trivial solutions are reflected as non-zero fixed points of Equations (21) or (20) and can be easily computed numerically by iteration. The macroscopic order parameter is given by the expected infection density ρ, computed as:

$$\rho = \frac{1}{N}\sum_{i=1}^{N} p_i \tag{22}$$

In **Figure 2**, the accuracy of the MMCA with respect to the HMF is shown by comparing the solutions obtained by both methods with the results of mechanistic Monte Carlo simulations.

4.1.1. Mathematical Analysis of the Convergence of the MMCA

According to the MMCA Equation (14), the evolution of the discrete dynamical system is dictated by iterating the map

$$F = (F_1, \dots, F_n) : \mathbb{R}^n \to \mathbb{R}^n \tag{23}$$

where, for $i = 1, 2, \dots, n$, and setting $\mathbf{p} = (p_1, p_2, \dots, p_n) \in \mathbb{R}^n$

$$F_i(\mathbf{p}) := 1 - \left(1 - (1 - \mu)p_i\right) q_i(\mathbf{p}) \text{ with}$$
$$q_i(\mathbf{p}) := \prod_{j=1}^{n}(1 - \beta r_{ij}p_j) \tag{24}$$

If $(p_1^0, \dots, p_n^0)$ represents the vector of initial conditions, then $(p_1^{k+1}, \dots, p_n^{k+1}) = F^k(p_1^0, \dots, p_n^0)$, where $F^k = F \circ F^{k-1}$. Given the problem's physical nature, F maps $[0, 1]^n$ into itself, thus restricting the study of the generated discrete dynamical system to the compact set $\Omega = [0, 1]^n$.

Numerical simulations[12] show that this kind of systems, governed by the map F, converge to an asymptotic distribution

$$\lim_{k\to\infty} F^k(\mathbf{p}) = \mathbf{p}^\infty = (p_1^\infty, \dots, p_n^\infty) \tag{25}$$

regardless on the initial condition $\mathbf{p} \in \Omega$.

© 2024 The Author(s). Annalen der Physik published by Wiley-VCH GmbH

15213889, 0, Downloaded from https://onlinelibrary.wiley.com/doi/10.1002/andp.202400078 by Universidad De Zaragoza, Wiley Online Library on [12/09/2024]. See the Terms and Conditions (https://onlinelibrary.wiley.com/terms-and-conditions) on Wiley Online Library for rules of use; OA articles are governed by the applicable Creative Commons License

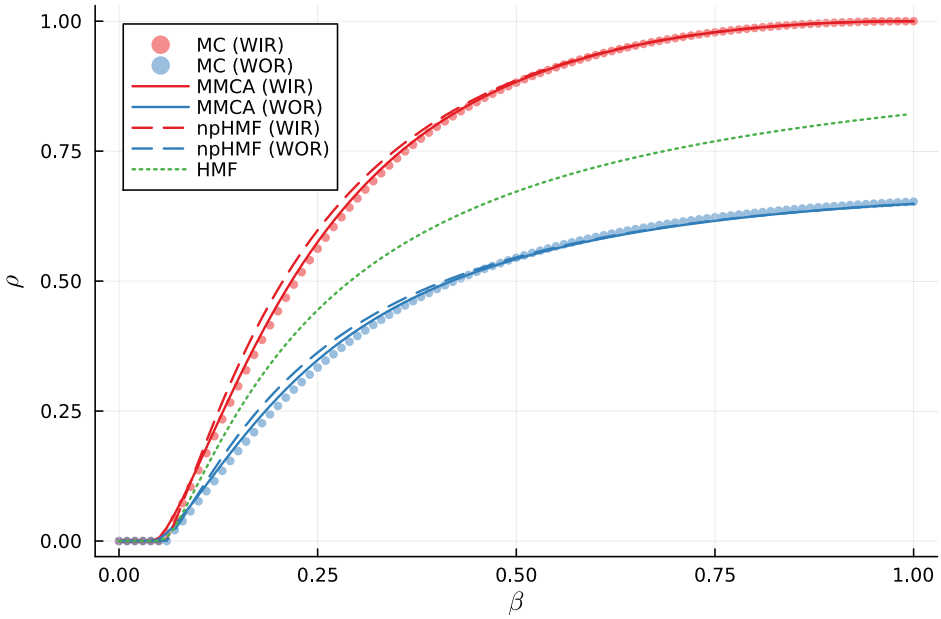

Figure 2. Agreement between Monte Carlo simulations and theoretical approaches for the SIS dynamic. The Monte Carlo simulations (MC, circles) are compared with the Microscopic Markov Chain Approach (MMCA, solid lines), the non-perturbative Heterogeneous Mean Field (npHMF, dashed lines), and the standard Heterogeneous Mean Field (HMF, dotted line). Simulations and models with (WIR, in red) and without (WOR, in blue) one-step reinfections; HMF (in green) is the same for both WIR and WOR variants of the SIS dynamic on networks. All results have been calculated for an SF network with 10^4 nodes and an exponent 2.7. The recovery probability is $\mu = 0.5$, and we have set $\rho_0 = 0.2$. HMF is solved by minimization of an error function since iteration diverges for most values of β, see ref. [29].

Therefore, a fixed point exists that acts as a global attractor for the discrete dynamical system in question. Numerical simulations also reveal that this global attractor $\mathbf{p}^\infty$ experiences a bifurcation at $\beta_0 := \frac{\mu}{\rho(R)}$, where $\rho(R)$ denotes the spectral radius of the matrix R.t is straightforward to confirm that the origin $\mathbf{0} = (0, \dots, 0)$ is a fixed point of F for any $\beta, \mu \in [0, 1]$. It is proved that for each $\mu \in (0, 1)$, this fixed point undergoes a *transcritical bifurcation* at the *epidemic threshold* $\beta_0 := \frac{\mu}{\rho(R)}$. Indeed, the origin is stable for $\beta < \beta_0$ and, as β approaches β_0, it collides with an unstable fixed point $\mathbf{z}_0$ originating from outside Ω. Consequently, for $\beta > \beta_0$, the origin becomes unstable, while $\mathbf{z}_0$ is stable and resides within Ω. This stability exchange due to the transcritical bifurcation elucidates, as it has been established,[30] that $\mathbf{0}$ is a global attractor for $\beta < \beta_0$ and $\mathbf{z}_0$ for $\beta > \beta_0$, i.e.,

$$\lim_{k\to\infty} F^k(\mathbf{p}) = \begin{cases} \mathbf{0} & \text{if } \beta < \beta_0, \\ \mathbf{z}_0 & \text{if } \beta > \beta_0, \end{cases} \quad \text{for all } \mathbf{p} \in \Omega \setminus \{\mathbf{0}\} \tag{26}$$

It was proved that the second-order phase transition toward the endemic phase is well captured by a transcritical transition of the dynamical system.[30] Exploiting the analysis of this transition it has been shown that the endemic state is stable and globally attracting for all values of the parameters beyond the critical transition. This result is essential to ground mathematically the numerical scenarios found by finite iterations of the model.

4.1.2. Recovering the Structure of the HMF Approach

As explained in Section 2, the heterogeneous mean–field (HMF) approach assumes that all nodes of the same degree behave equally. In terms of the MMCA formulation this means that $p_i = p_j$ if $k_i = k_j$, and the density ρ_k of infected nodes of degree k is given by

$$\rho_k = \frac{1}{N_k} \sum_{j \in K} p_j = p_i \,, \quad \forall i \in K \tag{27}$$

where K is the set of nodes with degree k, whose cardinality is denoted by N_k. This notation allows grouping together terms according to the degrees of the nodes. For instance, if the degree of node i is $k_i = k$, then

$$\sum_j a_{ji} p_j = \sum_{k'} \sum_{j \in K'} a_{ji} \rho_{k'} = \sum_{k'} \rho_{k'} \sum_{j \in K'} a_{ij} = \sum_{k'} \rho_{k'} C_{kk'} = k \sum_{k'} P(k'|k) \rho_{k'} \,, \tag{28}$$

where $C_{kk'} = kP(k'|k)$ is the expected number of links from a node of degree k to nodes of degree k'.

Substitution of the HMF approximation, Equation (27), into the MMCA equations leads to

WOR: $$\rho_k = (1 - \rho_k)(1 - q_k) + (1 - \mu)\rho_k \tag{29}$$

WIR: $$\rho_k = (1 - q_k) + (1 - \mu)\rho_k q_k \tag{30}$$

which can also be written as

WOR: $$0 = -\mu\rho_k + (1 - \rho_k)(1 - q_k) \tag{31}$$

© 2024 The Author(s). Annalen der Physik published by Wiley-VCH GmbH

15213889, 0, Downloaded from https://onlinelibrary.wiley.com/doi/10.1002/andp.202400078 by Universidad De Zaragoza, Wiley Online Library on [12/09/2024]. See the Terms and Conditions (https://onlinelibrary.wiley.com/terms-and-conditions) on Wiley Online Library for rules of use; OA articles are governed by the applicable Creative Commons License

WIR: $$0 = -\mu\rho_k + (1-(1-\mu)\rho_k)(1-q_k) \tag{32}$$

These equations constitute the HMF approximations of MMCA for the SIS model without and with reinfections, respectively.

We still need a HMF expression for q_k. For unweighted networks the value of q_i is

$$q_i = \prod_{j=1}^{N}(1-\beta r_{ji}p_j) = \prod_{j=1}^{N}\left(1-\beta a_{ji}R_\eta(k_j^{-1})p_j\right) \tag{33}$$

If node i has degree $k_i = k$, then

$$q_i = q_k = \prod_{k'}\prod_{j\in K'}\left(1-\beta a_{ji}R_\eta(k'^{-1})\rho_{k'}\right) \tag{34}$$

where we have grouped together the terms in the product by their degrees k' as in Equation (28). The expression within the parentheses is equal to 1 for all nodes of degree k' that are not connected to node i ($a_{ji}=0$), and equal to $[1-\beta R_\eta(k'^{-1})\rho_{k'}]$ for nodes of degree k' that are linked to i ($a_{ji}=1$). Besides, the expected number of such terms is $C_{kk'}$. Hence, we obtain

$$q_k = \prod_{k'}\left(1-\beta R_\eta(k'^{-1})\rho_{k'}\right)^{C_{kk'}} \tag{35}$$

Equations (31) and (32), together with Equation (35), form what is called the *Non-perturbative Heterogeneous Mean Field* (npHMF) equations of the SIS model in unweighted networks.[29] Note that in the derivation of the npHMF equations no assumption has been made about the proximity of the system to the epidemic threshold, where the epidemic prevalence is small, nor any linear approximation has been invoked, hence the qualification of "non-perturbative."

The solution of the npHMF equations follows the same steps as in MMCA, i.e., Equations (29), (30), and (35) are iterated until a fixed point (WIR, WOR) or a cycle (WOR) is found. As before, for the latter case, the average of oscillating values for the disease prevalence can be computed. Finally, the global epidemic prevalence is given by

$$\rho = \frac{1}{N}\sum_k N_k\rho_k\,. \tag{36}$$

It is easy to show that the standard HMF equations[22] are just a linear approximation of our WOR npHMF equations. Near the epidemic threshold β_c, where $\rho_k \ll 1$, we get

$$\begin{aligned} q_k &\sim 1-\beta\sum_{k'}C_{kk'}R_\eta(k'^{-1})\rho_{k'} \\ &= 1-\beta k\sum_{k'}P(k'|k)R_\eta(k'^{-1})\rho_{k'} \end{aligned} \tag{37}$$

which can be inserted into Equation (31) to give

$$0 = -\mu\rho_k + \beta k(1-\rho_k)\sum_{k'}P(k'|k)R_\eta(k'^{-1})\rho_{k'} \tag{38}$$

where

$$R_\eta(k'^{-1}) = \begin{cases} 1 & \text{for the RP,} \\ \dfrac{1}{k'} & \text{for the CP} \end{cases} \tag{39}$$

4.1.3. Epidemic Threshold

To complete this analysis, we review the derivation of the critical epidemic threshold using the different approaches here discussed. In ref. [12] it is shown that MMCA allows the determination of the epidemic threshold

$$\beta_c = \frac{\mu}{\Lambda_{max}(R)} \tag{40}$$

where $\Lambda_{max}(R)$ is the maximum eigenvalue of the matrix R of the contact probabilities r_{ij}. In particular,

$$\beta_c = \begin{cases} \dfrac{\mu}{\Lambda_{\max}(A)} & \text{for the RP,} \\ \mu & \text{for the CP} \end{cases} \tag{41}$$

These results are valid with and without reinfections, since at first order, Equations (16) and (17) coincide. In the same way, the critical points from npHMF Equations (31) and (32) are the same as in standard HMF, where the matrix H with elements $h_{kk'} = C_{kk'}R_\eta(k'^{-1})$ replaces matrix R,

$$\beta_c^{\mathrm{HMF}} = \frac{\mu}{\Lambda_{\max}(H)}\,, \tag{42}$$

with the well-known particular cases

$$\beta_c^{\mathrm{HMF}} = \begin{cases} \dfrac{\mu}{\Lambda_{\max}(C)} & \text{for the RP,} \\ \mu & \text{for the CP} \end{cases} \tag{43}$$

A comparison with Monte Carlo (MC) simulations reveals that MMCA yields a more accurate approximation of the epidemic threshold than HMF, preserving the integrity of the original network structure. Moreover, given the definition of contact probabilities, MMCA is adaptable to weighted and directed networks without necessitating adjustments to the equations, unlike HMF, which is constrained to networks that are neither weighted nor directed.

4.2. Microscopic Markov Chain Approach for Individual Links in Networks

So far we concentrated on introducing the MMCA to the modeling of epidemic spreading considering the states of nodes. A more accurate approach should consider the conditional probabilities of these states depending on the states of the neighbors.[31]

Let us introduce some notation to simplify the analysis. Denoting the previous joint probability as $\Phi_{ij} = P(\sigma_i = S, \sigma_j = I)$; the

© 2024 The Author(s). Annalen der Physik published by Wiley-VCH GmbH

15213889, 0, Downloaded from https://onlinelibrary.wiley.com/doi/10.1002/andp.202400078 by Universidad De Zaragoza, Wiley Online Library on [12/09/2024]. See the Terms and Conditions (https://onlinelibrary.wiley.com/terms-and-conditions) on Wiley Online Library for rules of use; OA articles are governed by the applicable Creative Commons License

higher the Φ_{ij}, the larger the likelihood that the disease propagates from node j to node i. It is worth mentioning that this feature is in general asymmetrical, meaning that the propagation of the illness can be more probable from j to i than the other way around. In the same way, the epidemic is restrained by edges where the nodes are in the same state, thus it is convenient to define the probabilities $\Theta^S_{ij} = P(\sigma_i = \sigma_j = S)$ and $\Theta^I_{ij} = P(\sigma_i = \sigma_j = I)$ for all pairs of neighboring nodes.

The evolution of the joint probability Φ_{ij} of one link depends on Φ, Θ^I and Θ^S to the rest of the neighboring links, and the infection rules of the SIS dynamics. Thus, the following equation for each link can be written:

$$\begin{aligned}\Phi_{ij}(t+1) = {} & \Theta^S_{ij}(t)\, q_{ij}(t)\,(1-q_{ji}(t)) \\ & + \Phi_{ij}(t)\,((1-\beta)q_{ij}(t))\,(1-\mu) \\ & + \Phi_{ji}(t)\,\mu\,(1-(1-\beta)q_{ji}(t)) \\ & + \Theta^I_{ij}(t)\,\mu(1-\mu)\end{aligned} \tag{44}$$

where all the possible changes of state of the nodes i and j are taken into account. The first term considers the probability that both nodes are in a susceptible state, and then node i remains susceptible while node j is infected by any of its other neighbors. The second term accounts for both nodes remaining in the same state, node i is not infected by any of its neighbors and node j is not recovered from the infection. Then, the third term represents the transition in which node i is infected and recovers while node j is susceptible and it is infected by any of its other neighbors. Finally, in the fourth term, both nodes are infected but node i recovers while node j does not. The asymmetry of probability Φ_{ij} multiplies the number of equations by two, since for each link between nodes i and j an equation for $\Phi_{ij}(t+1)$ and another for $\Phi_{ji}(t+1)$ are needed.

Similarly an expression for probability Θ^I_{ij} can be obtained as:

$$\begin{aligned}\Theta^I_{ij}(t+1) = {} & \Theta^S_{ij}(t)\,(1-q_{ij}(t))\,(1-q_{ji}(t)) \\ & + \Phi_{ij}(t)\,(1-(1-\beta)q_{ij}(t))\,(1-\mu) \\ & + \Phi_{ji}(t)\,(1-\mu)\,(1-(1-\beta)q_{ji}(t)) \\ & + \Theta^I_{ij}(t)\,(1-\mu)^2\end{aligned} \tag{45}$$

In this case there are only L equations, one per link, due to its symmetry. There is no need of extra equations for probability Θ^S_{ij} since the normalization leads to $\Theta^S_{ij} = 1 - \Phi_{ij} - \Phi_{ji} - \Theta^I_{ij}$.

The $q_{ij}(t)$ in Equations (44) and (45) stands for the probability that a susceptible node i is not infected by any of its neighbors (excluding node j):

$$q_{ij}(t) = \prod_{\substack{r=1 \\ r\neq j}}^{N} \left(1 - \beta A_{ri} h_{ir}\right) \tag{46}$$

where h_{ij} defines the hostility of j against i, i.e., the probability that node j is infected when node i is susceptible, $h_{ij} = P(\sigma_j = I | \sigma_i = S)$. The hostility can be obtained in terms of Θ^S_{ij} and Φ_{ij} as:

$$h_{ij} = \frac{\Phi_{ij}}{\Phi_{ij} + \Theta^S_{ij}} \tag{47}$$

Note that the denominator in Equation (47) is a property of node i given that $\Phi_{ij} + \Theta^S_{ij} = P(\sigma_i = S)$ for all neighboring nodes j of vertex i.

This system of $3L$ equations and unknowns is called the *Epidemic Link Equations* (ELE) model. It can be solved by iteration, starting from any meaningful initial condition, e.g., $\Theta^I_{ij}(0) = \rho_0^2$ and $\Phi_{ij}(0) = \Phi_{ji}(0) = \rho_0(1-\rho_0)$ (for any $0 < \rho_0 \leq 1$), until fixed values are found. Apart from the solution where all nodes are susceptible, $\Theta^S_{ij} = 1$ for all the links, a non-trivial one appears when the system is above the critical value of the epidemic spreading (see *Methods* for the analytic derivation of the epidemic threshold from ELE model). Finally, the incidence of the epidemic process, the average number of infected nodes in the whole system, can be computed as:

$$\rho = \frac{1}{N}\sum_{i=1}^{N}\frac{1}{k_i}\sum_{j=1}^{N} A_{ji}(\Phi_{ji} + \Theta^I_{ij}) \tag{48}$$

4.3. Microscopic Markov Chain Approach Beyond Pairwise Interactions

The interest in considering interactions beyond pairwise is a response to an actual necessity observed in complex systems. Behaviors, strategies, and conventions often require some form of reinforcement for their adoption.[32–37] The diffusion of these elements among individuals through learning and imitation can be studied as a contagion process.[38–41]

The MMCA's adaptation to accommodate interactions beyond pairwise focuses on analyzing triads, the simplest higher-order structure beyond pairs.[42] Let us start with the closure approximation applied to the exact microscopic equations on hypergraphs. Tracking the state evolution of subsets of nodes which form maximal cliques (i.e., cliques that are not subsets of larger ones) in the projection graph constructed by associating cliques to edges of the hypergraph. Accordingly, considering up to three-body interactions, the authors[42] account for the evolution of the state probability $P_i^{\sigma_i}$ for node i to be in state σ_i, $P_{ij}^{\sigma_i\sigma_j}$ for the maximal link ij to be in state $\sigma_i\sigma_j$, $P_{ijl}^{\sigma_i\sigma_j\sigma_l}$ for the (maximal) 3-clique ijl to be in state $\sigma_i\sigma_j\sigma_l$. Notice that a 3-clique, when projected back to the hypergraph, comes in one of three flavors: a length-3 cycle (or 3-cycle), conveying three two-body interactions, a 3-egde, conveying a three-body interaction, or a 2-simplex (or triangle), conveying all of them.

The state probability of other local structures is approximated in terms of the maximal cliques composing it. Considering random hypergraphs that are sparse to the extent that the probability for two maximal cliques to share more than one node vanishes in the infinite-size limit.[43] It thus needs a closure only for the following local structures: two connected maximal links, a maximal

© 2024 The Author(s). Annalen der Physik published by Wiley-VCH GmbH

15213889, 0, Downloaded from https://onlinelibrary.wiley.com/doi/10.1002/andp.202400078 by Universidad De Zaragoza, Wiley Online Library on [12/09/2024]. See the Terms and Conditions (https://onlinelibrary.wiley.com/terms-and-conditions) on Wiley Online Library for rules of use; OA articles are governed by the applicable Creative Commons License

link connected to a 3-clique, and two connected 3-cliques. Their state can be approximated as follows[42]:

$$P^{\sigma_i\sigma_j\sigma_l}_{\underline{ijl}} \approx \frac{P^{\sigma_i\sigma_j}_{ij} P^{\sigma_j\sigma_l}_{jl}}{P^{\sigma_j}_{j}} \tag{49}$$

$$P^{\sigma_i\sigma_j\sigma_l\sigma_h}_{\underline{ijlh}} \approx \frac{P^{\sigma_i\sigma_j}_{ij} P^{\sigma_j\sigma_l\sigma_h}_{jlh}}{P^{\sigma_j}_{j}} \tag{50}$$

$$P^{\sigma_i\sigma_j\sigma_l\sigma_h\sigma_k}_{\underline{ijlhk}} \approx \frac{P^{\sigma_i\sigma_j\sigma_l}_{ijl} P^{\sigma_l\sigma_h\sigma_k}_{lhk}}{P^{\sigma_l}_{l}} \tag{51}$$

where the underline indicates the shared node. Equations (46) are called a *triadic approximation*[44].

Introducing these closures in the MMCA equations gives a system that is difficult to analyze mathematically. To make the model analytically tractable, the authors[45] perform a mean-field approximation by regarding all the nodes and cliques as equivalent to their average counterparts. Accordingly, every node is assumed to be part of the same number of maximal links, $k^{(1)}$, 3-cliques, $k^{(1,0)}$, 3-edges, $k^{(0,1)}$, and triangles, $k^{(1,1)}$; and thus participates in $\kappa^{(1)} = k^{(1)} + 2(k^{(1,0)} + k^{(1,1)})$ two-body interactions and $\kappa^{(2)} = k^{(0,1)} + k^{(1,1)}$ three-body interactions. The state probabilities P^{σ}_{i}, $P^{\sigma\sigma'}_{ij}$ and $P^{\sigma\sigma'\sigma''}_{ijl}$, with $\sigma, \sigma', \sigma'' \in \{S, I\}$, are taken equal to their respective averages,

$$P^{\sigma} = \frac{1}{N}\sum_{i} P^{\sigma}_{i} \tag{52}$$

$$P^{\sigma\sigma'} = \frac{1}{Nk^{(1)}}\sum_{i,j} A^{(1)}_{ij} P^{\sigma\sigma'}_{ij} \tag{53}$$

and

$$P^{\sigma\sigma'\sigma''}_{x} = \frac{1}{2Nk^{x}}\sum_{i,j,l} A^{x}_{ijl} P^{\sigma\sigma'\sigma''}_{ijl} \tag{54}$$

the index $x \in \{(1,0),(0,1),(1,1)\}$ indicating the type of the considered 3-clique.[46]

Using the indicator function $\mathbb{1}_{p}$, giving 1 if condition p is fulfilled and 0 otherwise, the reduced system reads

$$\dot{P}^{I} = -P^{I} + \beta^{(1)} k^{(1)} P^{SI} + 2\beta^{(1)}\Big[k^{(1,0)}(P^{SSI}_{(1,0)} + P^{SII}_{(1,0)}) + k^{(1,1)}(P^{SSI}_{(1,1)} + P^{SII}_{(1,1)})\Big] + \beta^{(2)}\Big[k^{(0,1)} P^{SII}_{(0,1)} + k^{(1,1)} P^{SII}_{(1,1)}\Big] \tag{55}$$

$$\dot{P}^{SI} = -(1+\beta^{(1)})P^{SI} + P^{II} - \beta^{(1)}(k^{(1)}-1)P^{SI}\frac{P^{SI}-P^{SS}}{P^{S}} - \Big\{2\beta^{(1)}\Big[k^{(1,0)}(P^{SSI}_{(1,0)} + P^{SII}_{(1,0)}) + k^{(1,1)}(P^{SSI}_{(1,1)} + P^{SII}_{(1,1)})\Big] + \beta^{(2)}\Big[k^{(0,1)} P^{SII}_{(0,1)} + k^{(1,1)} P^{SII}_{(1,1)}\Big]\Big\}\frac{P^{SI}-P^{SS}}{P^{S}} \tag{56}$$

$$\begin{aligned}\dot{P}^{SSI}_{x} = {} & -2(1+\beta^{(1)}\mathbb{1}_{x\neq(0,1)})P^{SSI}_{x} + 2P^{SII}_{x} - \beta^{(1)}k^{(1)}P^{SI}\frac{2P^{SSI}_{x}-P^{SSS}_{x}}{P^{S}} \\ & - 2\beta^{(1)}\Big[(k^{(1,0)} - \mathbb{1}_{x=(1,0)})(P^{SSI}_{(1,0)} + P^{SII}_{(1,0)}) \\ & + (k^{(1,1)} - \mathbb{1}_{x=(1,1)})(P^{SSI}_{(1,1)} + P^{SII}_{(1,1)})\Big]\frac{2P^{SSI}_{x}-P^{SSS}_{x}}{P^{S}} \\ & - \beta^{(2)}\Big[(k^{(0,1)} - \mathbb{1}_{x=(0,1)})P^{SII}_{(0,1)} + (k^{(1,1)} - \mathbb{1}_{x=(1,1)})P^{SII}_{(1,1)}\Big] \\ & \times \frac{2P^{SSI}_{x}-P^{SSS}_{x}}{P^{S}}\end{aligned} \tag{57}$$

$$\begin{aligned}\dot{P}^{SII}_{x} = {} & -(2+2\beta^{(1)}\mathbb{1}_{x\neq(0,1)} + \beta^{(2)}\mathbb{1}_{x\neq(1,0)})P^{SII}_{x} + 2\beta^{(1)}\mathbb{1}_{x\neq(0,1)}P^{SSI}_{x} + P^{III}_{x} \\ & - \beta^{(1)}k^{(1)}P^{SI}\frac{P^{SII}_{x}-2P^{SSI}_{x}}{P^{S}} - 2\beta^{(1)}\Big[(k^{(1,0)} - \mathbb{1}_{x=(1,0)}) \\ & \times (P^{SSI}_{(1,0)} + P^{SII}_{(1,0)}) + (k^{(1,1)} - \mathbb{1}_{x=(1,1)})(P^{SSI}_{(1,1)} + P^{SII}_{(1,1)})\Big] \\ & \times \frac{P^{SII}_{x}-2P^{SSI}_{x}}{P^{S}} \\ & - \beta^{(2)}\Big[(k^{(0,1)} - \mathbb{1}_{x=(0,1)})P^{SII}_{(0,1)} + (k^{(1,1)} - \mathbb{1}_{x=(1,1)})P^{SII}_{(1,1)}\Big] \\ & \times \frac{P^{SII}_{x}-2P^{SSI}_{x}}{P^{S}}\end{aligned} \tag{58}$$

where $P^{S} = 1 - P^{I}$, $P^{SS} = 1 - P^{I} - P^{SI}$, $P^{II} = P^{I} - P^{SI}$, $P^{SSS} = 1 - P^{I} - P^{SII} - 2P^{SSI}$, $P^{III} = P^{I} - P^{SSI} - 2P^{SII}$.

This set of mean–field equations can be used to analytically determine the phase space of the system, and how the different parameters influence the corresponding transitions.[45] For a more accurate description of the system, the authors also introduce a Microscopic Epidemic Clique Equations (MECLE) model, which considers the state probabilities of the cliques in which the network can be decomposed.[42]

In **Figure 3**, we show a comparison between the prevalence ρ obtained using Monte Carlo (MC) simulations, the Microscopic Epidemic Clique Equations (MECLE) model, and the other discrete-time Markovian models, i.e., the simplicial ELE[47] and the original MMCA models. The generalization to larger structures is mathematically cumbersome, however, it is still possible to have a well-defined framework for groups, restricted to cliques of any size.

4.4. Microscopic Markov Chain Approach for Temporal Networks

Many phenomena emerge from the intricate interaction between the dynamics of spreading and the structural as well as temporal attributes of networks, posing challenges to their comprehensive understanding.

When analyzing spreading processes whose underlying topology is a complex network of human interactions, considering the potential changes in the network over time is crucial. Furthermore, in the case of epidemics, some containment strategies are specifically aimed at altering the network to reduce the spread.

© 2024 The Author(s). Annalen der Physik published by Wiley-VCH GmbH

15213889, 0, Downloaded from https://onlinelibrary.wiley.com/doi/10.1002/andp.202400078 by Universidad De Zaragoza, Wiley Online Library on [12/09/2024]. See the Terms and Conditions (https://onlinelibrary.wiley.com/terms-and-conditions) on Wiley Online Library for rules of use; OA articles are governed by the applicable Creative Commons License

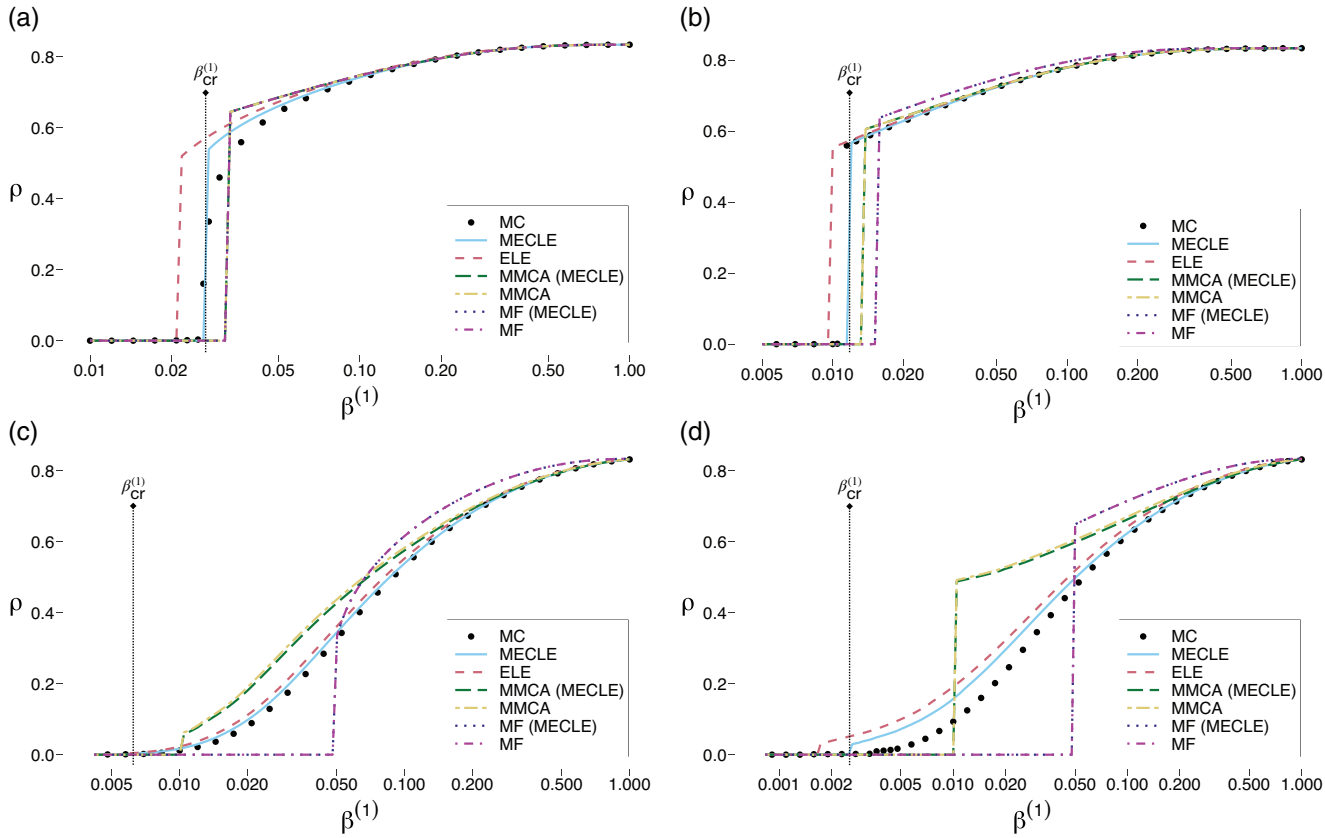

Figure 3. Comparison of pairwise and higher-order methods. Epidemic prevalence ρ as a function of the edge infection probability $\beta^{(1)}$ on different **2**D simplicial complexes (SCs). Results obtained from Monte Carlo (MC) simulations are depicted by dots, while lines represent the analytically computed prevalence using the indicated models. MMCA and MMCA(MECLE) refer to the Microscopic Markov Chain approximation of, respectively, the simplicial Epidemic Link Equations (ELE) model and the Microscopic Epidemic Clique Equations (MECLE) model, as obtained by considering the state probabilities of the nodes as uncorrelated; while MF and MF(MECLE) refer to their homogeneous mean–field approximations. Note that MF and MF(MECLE) are indistinguishable at the used scale. The value of the epidemic threshold, as computed in the MECLE is marked with a vertical dotted line. The recovery probability is fixed to $\mu = 0.2$. a) Periodic triangular SC with $\bar{k}^{(0,1)} = 0.00$, $\bar{k}^{(0,2)} = 0.00$, and $\bar{k}^{(1,2)} = 3.00$, being $\bar{k}^{(g,r)}$ the mean number of $(g, n+1)$-cliques incident on a node, and triangle infection probability $\beta^{(2)} = 0.25$; the relative error in locating the epidemic threshold is $\varepsilon_{\beta^{(1)}} \approx 0.08$ for MECLE and $\varepsilon_{\beta^{(1)}} \approx 0.12$ for ELE. b) Random SC with $\bar{k}^{(0,1)} = 4.10$, $\bar{k}^{(0,2)} = 0.00$ and $\bar{k}^{(1,2)} = 3.95$, and $\beta^{(2)} = 0.15$; $\varepsilon_{\beta^{(1)}} \approx 0.06$ for MECLE and $\varepsilon_{\beta^{(1)}} \approx 0.09$ for ELE. c) Dorogovtsev–Mendes SC with $\bar{k}^{(0,1)} = 1.10$, $\bar{k}^{(0,2)} = 0.00$ and $\bar{k}^{(1,2)} = 1.45$, and $\beta^{(2)} = 0.25$; $\varepsilon_{\beta^{(1)}} \approx 0.07$ for MECLE and $\varepsilon_{\beta^{(1)}} \approx 0.16$ for ELE. d) Same as (c) but with $\beta^{(2)} = 0.50$; $\varepsilon_{\beta^{(1)}} \approx 0.23$ for MECLE and $\varepsilon_{\beta^{(1)}} \approx 0.50$ for ELE. Reprinted with permission from Network clique cover approximation to analyze complex contagions through group interactions, by G. Burgio, A. Arenas, S. Gómez and J.T. Matamalas, Communications Physics 4, 111 (2021), see ref. [42].

The question that then arises is: how to adapt the MMCA framework to deal with a time-varying network structure? In ref. [48], the authors proposed a beautiful approach to address this challenge. The authors use a simple SIS propagation on a generic network with N nodes and adjacency matrix $\mathbf{A}$ given by the MMCA equations:

$$p_i^{(t)} = 1 - \left[1 - (1-\mu)p_i^{(t-1)}\right] \prod_j \left[1 - \beta A_{ji} p_j^{(t-1)}\right] \tag{59}$$

where $p_i^{(t)}$ is the probability for the node i to be in the infectious state at time t. They extend this paradigm to a temporal network by letting the adjacency matrix in Equation (59) depend on time:

$$p_i^{(t)} = 1 - \left[1 - (1-\mu)p_i^{(t-1)}\right] \prod_j \left[1 - \beta A_{ji}^{(t-1)} p_j^{(t-1)}\right] \tag{60}$$

Here $\mathbf{A}^{(t)}$ is the adjacency matrix associated with the t-the snapshot of the evolving network. In order to ensure the asymptotic solution of the SIS process in a generic temporal network assuming periodic boundary conditions for the network dynamics. Being T the total number of network time snapshots, the authors impose a closure, equivalent to periodic time boundary conditions, $\mathbf{A}^{(T+1)} \equiv \mathbf{A}^{(1)}$ that allows computation. As a consequence of the assumed periodic temporal dynamics of $A^{(t)}$, the asymptotic solution of Equation (60) is in principle periodic, with period T. Using a more convenient representation of the coupled dynamics the authors adopted the multi-layer approach introduced in ref. [49] Mapping the temporal network to a series of time snapshots (layers), that can be mathematically represented as a tensor space $\mathbb{R}^N \otimes \mathbb{R}^T$, where each node is identified by the pair of indices (i, t), corresponding to the node label, i, and the time frame, t, respectively. The ten-

© 2024 The Author(s). Annalen der Physik published by Wiley-VCH GmbH

15213889, 0, Downloaded from https://onlinelibrary.wiley.com/doi/10.1002/andp.202400078 by Universidad De Zaragoza, Wiley Online Library on [12/09/2024]. See the Terms and Conditions (https://onlinelibrary.wiley.com/terms-and-conditions) on Wiley Online Library for rules of use; OA articles are governed by the applicable Creative Commons License

sor representation of the obtained multilayer network is the following:

$$\mathbf{A}_{ij}^{tt'} = \delta^{t,t'+1}\left[\delta_{ij} + \mathbf{A}_{ij}^{(t)}\right] \tag{61}$$

Analogously to the definition of $\mathbf{A}$, one can also write in this representation the tensor associated to the SIS dynamics of Equation (60), coupling together contagion and network dynamics:

$$\mathbf{M}_{ij}^{tt'} = \delta^{t,t'+1}\left[(1-\mu)\delta_{ij} + \beta\mathbf{A}_{ij}^{(t)}\right] \tag{62}$$

The multi-layer representation and the definition of the tensor $\mathbf{M}$ introduces a simplified expression for Equation (60). The tensor space can be represented in single index notation through the isomorphism $\mathbb{R}^N \otimes \mathbb{R}^T \simeq \mathbb{R}^{NT}$. In other words, similar to the definition of the supra-adjacency matrix in ref. [49] it is possible to map $(i,t) \to \alpha = Nt + i$, with α running in $\{1,\ldots,NT\}$, allowing us to write the network tensor $\mathbf{M}$ in matrix form

$$\mathbf{M} = \begin{pmatrix} 0 & 1-\mu+\beta A^{(1)} & 0 & \cdots & 0 \\ 0 & 0 & 1-\mu+\beta A^{(2)} & \cdots & 0 \\ \vdots & \vdots & \vdots & \vdots & \vdots \\ 0 & 0 & 0 & \cdots & 1-\mu+\beta A^{(T-1)} \\ 1-\mu+\beta A^{(T)} & 0 & 0 & \cdots & 0 \end{pmatrix} \tag{63}$$

$\mathbf{M}$ provides a network representation of the topological and temporal dimensions underlying the dynamics of Equation (60), that here are interrelated and flattened. Its directed nature preserves the causality of the process, while its weights account for the SIS transition probabilities. The Markov process is now described by a trajectory in $\mathbb{R}^{NT}$ where the state vector $\hat{p}_\alpha(\tau)$ represents the probability of each node to be infected at each time step t included in the interval $[\tau T, (\tau+1)T]$. Consistently, Equation (60) becomes

$$\hat{p}_\alpha(\tau) = 1 - \prod_\beta \left[1 - M_{\beta\alpha}\hat{p}_\beta(\tau - 1)\right] \tag{64}$$

Given that vector $\hat{p}$ encodes a 1-period configuration, the T-periodic asymptotic state of the SIS process is now mapped into the steady state $\hat{p}_\alpha(\tau) = \hat{p}_\alpha(\tau - 1)$. The latter can be recovered as the solution of the equilibrium equation:

$$\hat{p}_\alpha = 1 - \prod_\beta \left(1 - M_{\beta\alpha}\hat{p}_\beta\right) \tag{65}$$

that is formally the same as the stationary condition imposed on Equation (59) for the static network case, and is similar to the Markov chain approaches used to solve contagion processes in multiplex and interconnected networks.[10,50,51]

5. Microscopic Markov Chain Approach of Interacting Spreading Processes

Frequently, various dynamical processes operate concurrently within a system of interacting agents, necessitating consideration of these interactions when determining the system's state. For instance, the outcome of an epidemic is not isolated from other processes, such as information diffusion. Human behavior plays a pivotal role in accurately predicting the outcome of an epidemic, particularly in diseases transmitted directly. To address this critical issue within the existing framework, we will explore various contributions in this area. Throughout this section, we will employ the theory of multilayer networks to guide our discussion.[49,52,53]

Intertwined dynamical processes represent a category of dynamics where the multilayer structure plays a pivotal role. To date, the most extensively examined instances include coupled spreading processes, which are fundamental to comprehending phenomena like the concurrent spreading of two diseases within networks[50,54–57] and the intertwined spread of disease with the dissemination of information or behaviors.[10,58–61] We highlight two primary effects: 1) two spreading processes can mutually enhance each other (for example, one disease facilitating the infection by another,[55]) and 2) one process can impede the spread of the other (for instance, one disease can prevent infection by another disease,[55] or the spread of awareness about a disease can limit the disease's transmission.[10]) Interacting spreading processes also manifest other intriguing dynamics, with multilayer networks offering a fitting framework to investigate these phenomena.[58]

5.1. Spreading of Information and Epidemics

Let us start by defining the specific setup analyzed in ref. [10, 61] Using a multiplex, with different connectivity at each layer, corresponding to the layer of *physical* persistent social contacts (those that can infect you), and to the layer of *virtual* contacts (those that communicate with you but are not necessarily in physical contact, e.g., Facebook friends, etc.). Note that the actors in both layers are the same. However, as observed in interdependent networks[62] the interrelation between two different structures is responsible for the emergence of new physical effects on the epidemic onset and prevalence of the epidemics.

On top of the virtual network where the UAU process takes place, nodes spread awareness of the epidemics. The states in this process are unaware (U), and aware (A) of the existence of the epidemics and their prevention. Unaware individuals do not have information about how to prevent infection, while aware individuals reduce their risk to be infected. Awareness can come from two sources, communication with aware neighbors (becoming aware with a probability λ) or because the individual is already infected. Since the awareness corresponds to cycles parallel to the seasonality of the epidemics, there is a certain probability of an individual to forget the awareness or not to care about it, and become again, at all effects, unaware (with a probability δ). See **Figure 4** for a sketch of this process.

In the physical layer, the nodes are susceptible (S) or infected (I). The infection propagates from certain infected individuals to their neighbors with a probability β, and infected nodes eventually recover with probability μ. After an individual gets infected it is automatically aware of the infection and changes its state in the virtual contact layer. On the other hand, if an individual is aware of the virtual layer and is susceptible to the physical layer, it reduces its own infectivity by a factor γ. Here, it is worth distinguishing between the original unaware infectivity β^U and the subsequent infectivity after being aware of the infection $\beta^A = \gamma\beta^U$. In the particular case of $\gamma = 0$, the aware individuals are completely immune to the infection.

According to this scheme, an individual can be in three different states: unaware and susceptible (US), aware and susceptible (AS) or aware and infected (AI). Note that the state unaware and infected (UI) is spurious because, according to the definition of

© 2024 The Author(s). Annalen der Physik published by Wiley-VCH GmbH

15213889, 0, Downloaded from https://onlinelibrary.wiley.com/doi/10.1002/andp.202400078 by Universidad De Zaragoza, Wiley Online Library on [12/09/2024]. See the Terms and Conditions (https://onlinelibrary.wiley.com/terms-and-conditions) on Wiley Online Library for rules of use; OA articles are governed by the applicable Creative Commons License

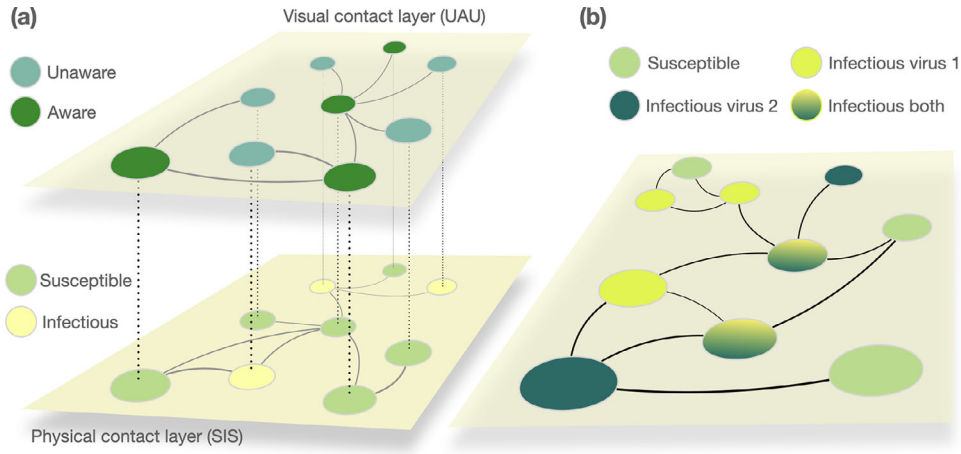

Figure 4. Sketch of two types of intertwined dynamical processes. a) Represents the interplay of information and epidemic spreading in a multiplex layer. The visual contact layer, where information diffuses, and the physical contact layer, where the epidemics evolve), are depicted. In the former, states are represented as U (Unaware) and A (Aware). For the physical layer, the standard states of the SIS model are presented: S (Susceptible) and I (Infected) individuals. b) Represents the spread of two interacting viruses in a contact network. Both pathogens spread across the same contact network and nodes can take four states: Susceptible, infectious of either virus 1 or 2, and infectious of both pathogens.

the dynamical process stated, it becomes immediately (AI). The MMCA equations for the coupled dynamics in the multiplex are derived using the total probability of the different states.

Let us denote a_{ij} and b_{ij} the adjacency matrices that support the UAU and the SIS processes, respectively. Every node i has a certain probability of being in one of the three states at time t, denoted by $p_i^{\mathrm{AI}}(t)$, $p_i^{\mathrm{AS}}(t)$, and $p_i^{\mathrm{US}}(t)$ respectively. Assuming the absence of dynamical correlations,[22] the transition probabilities for node i not being informed by any neighbors $r_i(t)$, not being infected by any neighbors if i was aware $q_i^{\mathrm{A}}(t)$, and not being infected by any neighbors if i was unaware $q_i^{\mathrm{U}}(t)$ are

$$
\begin{aligned}
r_i(t) &= \prod_j (1 - a_{ji} p_j^{\mathrm{A}}(t)\lambda) \\
q_i^{\mathrm{A}}(t) &= \prod_j (1 - b_{ji} p_j^{\mathrm{AI}}(t)\beta^{\mathrm{A}}) \\
q_i^{\mathrm{U}}(t) &= \prod_j (1 - b_{ji} p_j^{\mathrm{AI}}(t)\beta^{\mathrm{U}})
\end{aligned} \tag{66}
$$

where $p_j^{\mathrm{A}} = p_j^{\mathrm{AI}} + p_j^{\mathrm{AS}}$. Using Equation (66) one can develop the Microscopic Markov Chains for the coupled processes for each node i as

$$
p_i^{\mathrm{US}}(t+1) = p_i^{\mathrm{AI}}(t)\delta\mu + p_i^{\mathrm{US}}(t) r_i(t) q_i^{\mathrm{U}}(t) + p_i^{\mathrm{AS}}\delta q_i^{\mathrm{U}}(t) \tag{67}
$$

$$
\begin{aligned}
p_i^{\mathrm{AS}}(t+1) = {} & p_i^{\mathrm{AI}}(t)(1-\delta)\mu + p_i^{\mathrm{US}}(1 - r_i(t)) q_i^{\mathrm{A}}(t) \\
& + p_i^{\mathrm{AS}}(t)(1-\delta) q_i^{\mathrm{A}}(t)
\end{aligned} \tag{68}
$$

$$
\begin{aligned}
p_i^{\mathrm{AI}}(t+1) = {} & p_i^{\mathrm{AI}}(t)(1-\mu) + p_i^{\mathrm{US}}\Big[(1 - r_i(t))(1 - q_i^{\mathrm{A}}(t)) \\
& + r_i(t)(1 - q_i^{\mathrm{U}}(t))\Big] \\
& + p_i^{\mathrm{AS}}(t)\Big[\delta(1 - q_i^{\mathrm{U}}(t)) + (1-\delta)(1 - q_i^{\mathrm{A}}(t))\Big]
\end{aligned} \tag{69}
$$

By iteratively solving the aforementioned equations, the authors demonstrate how the evolution of epidemics and the flow of information about awareness significantly alter our understanding of epidemic dynamics in more realistic settings.

A comprehensive generalization is presented in ref. [63] where the authors' model encompasses all transitions deemed plausible for both disease contagion processes and rumor propagation. The model is demonstrated to encapsulate not only conventional spreading mechanisms but also integrates critical attributes pertinent to social dynamics, including apathy, the phenomenon of forgetting, and the fluctuation of interest levels.

5.2. Competing Spreading Processes

A prototypical example of competing spreading processes involves the interaction between multiple pathogens spreading across networks that connect a given set of nodes. An outbreak of a first pathogen that provides immunity to another, subsequently spreading on a second network connecting the same set of nodes, is most effective when the degrees of connectivity in the two networks are positively correlated. Conversely, if the degrees are uncorrelated or negatively correlated, increasing heterogeneity diminishes the capacity of the first process to prevent the second one from reaching epidemic proportions.[64]

The MMCA formulation for this novel setup is detailed in ref. [61, 65, 66] employing a methodology similar to that outlined in the preceding section. This formulation accommodates the state transitions from unaware to aware, which, in the context of two diseases, parallels the transition from susceptible to infected for a second disease. Within this framework, the two dynamical processes have the potential to either enhance each other's prevalence or inhibit the spread of one disease by the other.[67]

Start by assuming that contagion processes are dictated by an unweighted and undirected contact network of N nodes, each

© 2024 The Author(s). Annalen der Physik published by Wiley-VCH GmbH

15213889, 0, Downloaded from https://onlinelibrary.wiley.com/doi/10.1002/andp.202400078 by Universidad De Zaragoza, Wiley Online Library on [12/09/2024]. See the Terms and Conditions (https://onlinelibrary.wiley.com/terms-and-conditions) on Wiley Online Library for rules of use; OA articles are governed by the applicable Creative Commons License

representing an agent, with interactions determined by the L links of the network. The network is described by its adjacency matrix $\mathbf{A}$, whose entries are defined as $A_{ij} = 1$ if nodes i and j are connected and $A_{ij} = 0$ otherwise. For the spreading dynamics, each disease α can be individually modeled by a Susceptible-Infected-Susceptible (SIS) framework, where the contagion and recovery probabilities are denoted by p_α and r_α, respectively. In the absence of other pathogens, each disease α spreads from an infected agent to a susceptible one with probability p_α, while infected agents revert to being susceptible with probability r_α. Here, for the sake of simplicity, restricting the analysis to the case of two interacting diseases, such that $\alpha = 1, 2$. The interaction between the two diseases requires coupling two SIS dynamics. Consequently, agents subjected to a double SIS dynamic can be in one of four possible states: susceptible to both diseases (SS), infected by the first disease and susceptible to the second (IS), susceptible to the first and infected by the second (SI), and infected by both pathogens (II).

The authors describe the transitions governing the two coupled SIS dynamics, i.e., defining the transition probabilities between the four epidemic states previously mentioned. Initially, for healthy (SS) agents, it is considered that the probability of being infected with pathogen α is not affected by the presence of the other. Therefore, both pathogens are transmitted to SS agents with probabilities p_1 and p_2, respectively. To apply the authors' model to mutually exclusive diseases, double contagions of fully susceptible agents are forbidden.

The interaction between both circulating diseases is incorporated via a scaling parameter, q, affecting the probability that an agent already infected by one disease catches the other one. Thus, $q < 1$ implies that agents infected by one disease are less likely to get the other one, encoding a competition between both diseases. Conversely, $q > 1$ suggests that being affected by one disease boosts the contagion by the other, corresponding to a cooperative regime. Finally, all recovery processes are assumed to be independent of the circulation of other pathogens, so that individuals overcome diseases 1 and 2 with probabilities r_1 and r_2, respectively.

Mathematically, the formalism developed by the authors comprises a set of interdependent Markovian equations enabling the tracking of the temporal evolution of the dynamical state of each agent i. Since there are four possible epidemic states for each of the N agents, $3N$ equations are required to completely characterize the evolution of the network. Given an agent, say i, the authors denote as $[\rho^\gamma]_i^t$ the probability that this agent belongs to each of the following states γ ($\gamma = IS, SI, II$) at time t. Under the microscopical rules defined above, the temporal evolution of these probabilities is as follows:

$$[\rho^{II}]_i^{t+1} = [\rho^{SI}]_i^t (1-r_2)\left(1-\prod_j^N\left[1-A_{ij}p_1 q\left([\rho^{IS}]_j^t+[\rho^{II}]_j^t\right)\right]\right) + [\rho^{IS}]_i^t (1-r_1)\left(1-\prod_j^N\left[1-A_{ij}p_2 q\left([\rho^{SI}]_j^t+[\rho^{II}]_j^t\right)\right]\right) + [\rho^{II}]_i^t (1-r_1)(1-r_2) \tag{70}$$

$$[\rho^{IS}]_i^{t+1} = [\rho^{SI}]_i^t \left[r_2\left(1-\prod_j^N\left[1-A_{ij}p_1 q([\rho^{IS}]_j^t+[\rho^{II}]_j^t)\right]\right)\right] + [\rho^{IS}]_i^t (1-r_1)\prod_j^N\left[1-A_{ij}p_2 q([\rho^{SI}]_j^t+[\rho^{II}]_j^t)\right] + [\rho^{II}]_i^t r_2 (1-r_1) + \left[\rho^{SS}\right]_i^t\left(1-\prod_j^N\left[1-A_{ij}\left(p_1([\rho^{IS}]_j^t+[\rho^{II}]_j^t)+p_2([\rho^{SI}]_j^t + [\rho^{II}]_j^t) - p_1p_2[\rho^{II}]_j^t\right)\right]\right) f_{IS} \tag{71}$$

$$[\rho^{SI}]_i^{t+1} = [\rho^{IS}]_i^t \left[r_1\left(1-\prod_j^N\left[1-A_{ij}p_2 q([\rho^{SI}]_j^t+[\rho^{II}]_j^t)\right]\right)\right] + [\rho^{SI}]_i^t (1-r_2)\prod_j^N\left[1-A_{ij}p_1 q([\rho^{IS}]_j^t+[\rho^{II}]_j^t)\right] + [\rho^{II}]_i^t r_1 (1-r_2) + \left[\rho^{SS}\right]_i^t\left(1-\prod_j^N\left[1-A_{ij}\left(p_1([\rho^{IS}]_j^t+[\rho^{II}]_j^t)+p_2([\rho^{SI}]_j^t + [\rho^{II}]_j^t) - p_1p_2[\rho^{II}]_j^t\right)\right]\right) f_{SI} \tag{72}$$

For the sake of readability, the variable $\left[\rho^{SS}\right]_i^t$ is included, whose value is automatically calculated as $1 - \left[\rho^{IS}\right]_i^t - \left[\rho^{SI}\right]_i^t - \left[\rho^{II}\right]_i^t$. Note that the contagion processes involving totally susceptible (SS) agents are influenced by f_{IS} and f_{SI}. These factors represent the probability of contracting one disease when exposed to the other pathogen. To define this probability, a rule is established for the scenario in which a fully susceptible agent is in contact with both pathogens when interacting with its neighbors. Here, each disease will be contracted with the same probability. Accordingly, the probabilities f_{IS} and f_{SI} are defined as:

$$f_{IS} = \frac{g_{IS}(1-0.5g_{SI})}{g_{IS}(1-0.5g_{SI}) + g_{SI}(1-0.5g_{IS})} \tag{73}$$

$$f_{SI} = \frac{g_{SI}(1-0.5g_{IS})}{g_{IS}(1-0.5g_{SI}) + g_{SI}(1-0.5g_{IS})} \tag{74}$$

where g_{IS} and g_{SI} are the probabilities of making at least one infectious contact with individuals affected by the first and the second disease, respectively. These probabilities are expressed as:

$$g_{IS} = 1 - \prod_j^N\left[1-A_{ij}p_1\left([\rho^{IS}]_j^t+[\rho^{II}]_j^t\right)\right] \tag{75}$$

© 2024 The Author(s). Annalen der Physik published by Wiley-VCH GmbH

15213889, 0, Downloaded from https://onlinelibrary.wiley.com/doi/10.1002/andp.202400078 by Universidad De Zaragoza, Wiley Online Library on [12/09/2024]. See the Terms and Conditions (https://onlinelibrary.wiley.com/terms-and-conditions) on Wiley Online Library for rules of use; OA articles are governed by the applicable Creative Commons License

$$g_{SI} = 1 - \prod_{j}^{N} \left[1 - A_{ij} p_2 \left([\rho^{SI}]_j^t + [\rho^{II}]_j^t \right)\right] \tag{76}$$

With these equations, the authors complete the Markovian description for two interacting diseases. The extension to more interacting diseases will follow the same strategy presented here, but accounting for more parameters of interaction.

6. Microscopic Markov Chain Approach to Metapopulation Dynamics

A critical inquiry pertains to the applicability of the MMCA beyond contacts networks, e.g., when the mutual interactions between agents (contacts with infected neighbors) is complemented by their spatial spread (mobility) as a second driver of the onset of epidemic outbreaks. To address the geographical spread of diseases one should rely on metapopulation frameworks that allow to formulate reaction-diffusion models in which the MMCA can offer useful insights and, as we show below, can be empirically validated during real epidemic scenarios.

Over the past decade, the exploration of metapopulation dynamics has embarked on a quest to bridge the gap toward the realism of mechanistic simulations,[68] progressively embedding a more comprehensive understanding of human behavior and mobility patterns.[69,70] The pioneering efforts in this realm, marked by the intricate analysis of human mobility networks,[71–74] have consistently highlighted the significance of the recurrent nature of human movements, especially pertinent at urban and regional scales.[75–80] These insights have not only enhanced our grasp of mobility's complexity but also underscored its critical role in shaping interactions within and across communities.[81–83]

In response to these challenges, the MMCA has been instrumental to tackle the analysis of a family of metapopulation models that aim at capturing human flows especially at urban or regional scales. Here we summarize the main framework of these models as well as their application to the dynamics of SARS-CoV-2 epidemics. For a complete review on the subject we refer to ref. [84].

6.1. The Basic MIR Model

In the context of epidemic spreading at urban or regional scales, it is essential to consider the recurrent nature of human mobility, as it plays a critical role in shaping the patterns of interaction and disease spread within and between communities. The characterization of these mobility patterns is effectively accomplished through the use of Origin–Destination (OD) matrices, which serve as a quantitative framework for understanding the daily movements of individuals across different subpopulations or patches within a metapopulation.

The former recurrent mobility patterns can be accurately modeled by the so-called Movement-Interaction-Return (MIR) model.[85] This model assigns each individual to a home subpopulation and models their daily movements through a three-stage process within each time step: diffusion, where individuals decide to move to a different patch or stay in their residential patch with probability p_d; reaction, involving interactions between individuals present in the same subpopulation at time t; and return, where individuals who moved return to their original subpopulations, incorporating household-level interactions as highlighted by Granell and Mucha.[86] This framework allows us to differentiate between daytime (D) and nighttime (N) interactions, including those with household members.

The formalism of the MIR model leverages the OD matrix to delineate the mobility flows within a metapopulation, further enriched by demographic data from each subpopulation. This setup enables the development of MMCA equations that capture the evolution of the epidemic compartments across patches. In the case of the SIS dynamics, the MIR model is then characterized by the evolution of the infection probabilities across the patches $\{\rho_i(t)\}$, encapsulated in the equations:

$$\rho_i(t+1) = (1-\mu)\rho_i(t) + (1-\rho_i(t))\Pi_i(t) \tag{77}$$

where $\Pi_i(t)$ is the probability that a resident of patch i becomes infected at time t:

$$\Pi_i(t) = (1-p_d)\left[P_i^D(t) + (1-P_i^D(t))P_i^N(t)\right] + p_d \sum_{j=1}^{N} R_{ij}\left[P_j^D(t) + (1-P_j^D(t))P_i^N(t)\right] \tag{78}$$

The former expression effectively separates the probability of infection into two distinct scenarios: one where the infection occurs within an individual's home patch i, and another where the infection takes place in a different patch j. The relative likelihood of these events is determined by the parameters $(1-p_d)$ and p_d, respectively. Thus, p_d represents the crucial parameter for modulating the extent of spatial movement and, consequently, the spread of the disease across patches. Moreover, the computation of the second term in the r.h.s. leverages the $\mathbf{R}$ matrix in which each element R_{ij} signifies the probability that an individual, originally from patch i, visits patch j. This $\mathbf{R}$ matrix, derived from the Origin–Destination (OD) matrix with entries $R_{ij} = n_{ij}/\sum_l n_{il}$, adheres to the properties of a row stochastic matrix, ensuring that the sum of probabilities for all possible destinations from any given patch equals one, i.e., $\sum_{j=1}^{N} R_{ij} = 1$ for all i. Thus, in this context the MMCCA framework not only facilitates a realistic representation of movement patterns within the population but also enables precise modulation of the system's spatial dynamics through p_d.

Finally, in Equation (78) the probability of infection at any given location during the day (denoted as D) and within households at night (denoted as N) is represented by two distinct sets of probabilities, $P_i^D(t)$ and $P_i^N(t)$. These probabilities, crucial for understanding the spread of infection, are given by the following equations:

$$P_i^D(t) = 1 - \left(1 - \beta \frac{I_i^{\text{eff}}(t)}{n_i^{\text{eff}}}\right)^{z^D f_i} \tag{79}$$

$$P_i^N(t) = 1 - \left(1 - \beta\rho_i(t)\right)^{z^N \sigma_i} \tag{80}$$

where, as usual in this review, β is the disease's transmission probability per contact. These equations account for interactions

© 2024 The Author(s). Annalen der Physik published by Wiley-VCH GmbH

15213889, 0, Downloaded from https://onlinelibrary.wiley.com/doi/10.1002/andp.202400078 by Universidad De Zaragoza, Wiley Online Library on [12/09/2024]. See the Terms and Conditions (https://onlinelibrary.wiley.com/terms-and-conditions) on Wiley Online Library for rules of use; OA articles are governed by the applicable Creative Commons License

that occur outside the household during the day and those within households at night. The effective number of infected individuals (I_i^{eff}) and the effective population (n_i^{eff}) in a patch after mobility phases are factored into these probabilities, and are defined as:

$$n_i^{\text{eff}} = \sum_{j=1}^{N} \left[(1-p_d)\delta_{ij} + p_d R_{ji}\right] n_j \tag{81}$$

$$I_i^{\text{eff}} = \sum_{j=1}^{N} \left[(1-p_d)\delta_{ij} + p_d R_{ji}\right] n_j \rho_j(t) \tag{82}$$

Equipped with these two quantities one can compute the probability of finding an infectious individual in patch i as the ration $I_i^{\text{eff}}(t)/n_i^{\text{eff}}$, as used in Equation (79). Finally, Equations (79) and (80) compute the total number of contacts during daytime ($z^D f_i$) and the number of contacts within households at night ($z^N \sigma_i$) respectively. Here, f_i relates to the density of the population in a patch, and σ_i reflects the average household size in patch i. These metrics are key for capturing the variability in contact patterns among different patches.

Beyond the agreement of the MMCA formulation of the MIR model with mechanistic simulations, the model delineates an analytical expression for the epidemic threshold, determined after the linear stability analysis of the disease-free equilibrium and with the following expression

$$\lambda_c = \frac{\mu}{\Lambda_{max}(\boldsymbol{M})} \tag{83}$$

where $\Lambda_{max}(\boldsymbol{M})$ represents the maximum eigenvalue of a matrix $\boldsymbol{M}$ called the mixing matrix whose (i,j) entry reads:

$$\begin{aligned} M_{ij} = \Bigg[& \left((1-p_d)^2 \frac{z^D f_i}{n_i^{\text{eff}}} + \frac{z^N \sigma_i}{n_i} \right) \delta_{ij} \\ & + p_d(1-p_d) \left(R_{ji} \frac{z^D f_i}{n_i^{\text{eff}}} + R_{ij} \frac{z^D f_j}{n_j^{\text{eff}}} \right) \\ & + p_d^2 \sum_{l=1}^{N} R_{il} R_{jl} \frac{z^D f_l}{n_l^{\text{eff}}} \Bigg] n_j \end{aligned} \tag{84}$$

The mixing matrix is a central object since it encapsulates the three fundamental interactions through which individuals from patches i and j engage with one another, each being modulated by the mobility parameter p_d. In this regard, a particularly innovative aspect of this approach emerges in the analysis of how the epidemic threshold is influenced by the mobility parameter p_d. Contrary to initial expectations, it is observed that higher mobility can actually contribute to reducing the overall prevalence of the epidemic, thereby elevating the threshold required for an epidemic to sustain itself. This intriguing outcome, called *epidemic detriment by mobility*,[85,87] arises from the model's ability to accurately reflect the diverse demographic structures of real-world urban and regional settings, along with the specific patterns of commuting that characterize human mobility.

The model reviewed here is the simplest version of a family of models to capture different ingredients that are not included in the original formulation. The generalization to multiplex metapopulations,[88] the inclusion of heterogeneous visit times[89] and contact patterns[90] at destinations, or the ability to distinguish residents of each metapopulation according to their usual destination.[91] These and other refinements to the MMCA of the MIR metapopulation model can be consulted in the recent review.[84]

6.2. Application to Real-World Epidemics

Among the insights that the MIR model offers to disentangle the influence of mobility to the onset of the epidemic, the analytical expression of the epidemic threshold provided by the MMCA is essential for identifying the conditions under which an epidemic can propagate through a metapopulation, thereby guiding the development of strategic interventions and containment measures.

The direct application of the MMCA to MIR models, specially tailored for particular communicable diseases and epidemic interventions, has proven useful and informative to health authorities. Importantly, the Markovian framework adapted to the unique transmission dynamics of the disease in question, has been instrumental in assessing the progression and impact of epidemics, including COVID-19 across various countries[92–94] and dengue.[95,96] Likewise, the MIR model has been leveraged to enhance the efficiency of resource distribution in epidemic control efforts,[97] such as employing Wolbachia-infected mosquitoes to combat dengue,[98] and in evaluating the significant role of individual[99] and collective[100] awareness in disease mitigation.

To illustrate how the basic MMCA formulation of the MIR model can be adapted to study specific diseases, let's consider its application to SARS-CoV-2 transmission analysis.[92] In terms of transmission, the model accounted for the significant role of asymptomatic infections, which constitute $\approx 40\%$[101] of cases, in the concealed spread of the disease during its early stages. This covert spread leads to a delayed enactment of containment measures, which are traditionally based on the observed incidence of symptomatic cases. From a clinical perspective, the model considers the extended hospitalization durations required by severe cases, particularly those necessitating intensive care unit (ICU) admission, as the saturation of these facilities poses a major political and healthcare challenge during COVID-19 epidemics.

To synthesize this knowledge within a unified framework, the authors develop an epidemiological model featuring ten compartments that delineate the epidemiological and clinical statuses of individuals across different patches within the metapopulation. Moreover, the model segregates these compartments into three age strata—youth, adults, and older adults—to reflect the epidemiological, clinical, and behavioral disparities among these groups. Importation and exportation events of SARS-CoV-2 between patches are predominantly attributed to the mobility of the active population. Conversely, the clinical progression of COVID-19 varies significantly across age groups,[102–104] with infections in younger individuals often resulting in negligible or mild symptoms,[105] whereas older individuals tend to develop severe symptoms necessitating hospitalization.

The intricate structure of the metapopulation model enables the authors to design and assess the efficacy of containment strategies aimed at halting the spread of SARS-CoV-2. Specifically, the model concentrates on policies that employ global or

© 2024 The Author(s). Annalen der Physik published by Wiley-VCH GmbH

15213889, 0, Downloaded from https://onlinelibrary.wiley.com/doi/10.1002/andp.202400078 by Universidad De Zaragoza, Wiley Online Library on [12/09/2024]. See the Terms and Conditions (https://onlinelibrary.wiley.com/terms-and-conditions) on Wiley Online Library for rules of use; OA articles are governed by the applicable Creative Commons License

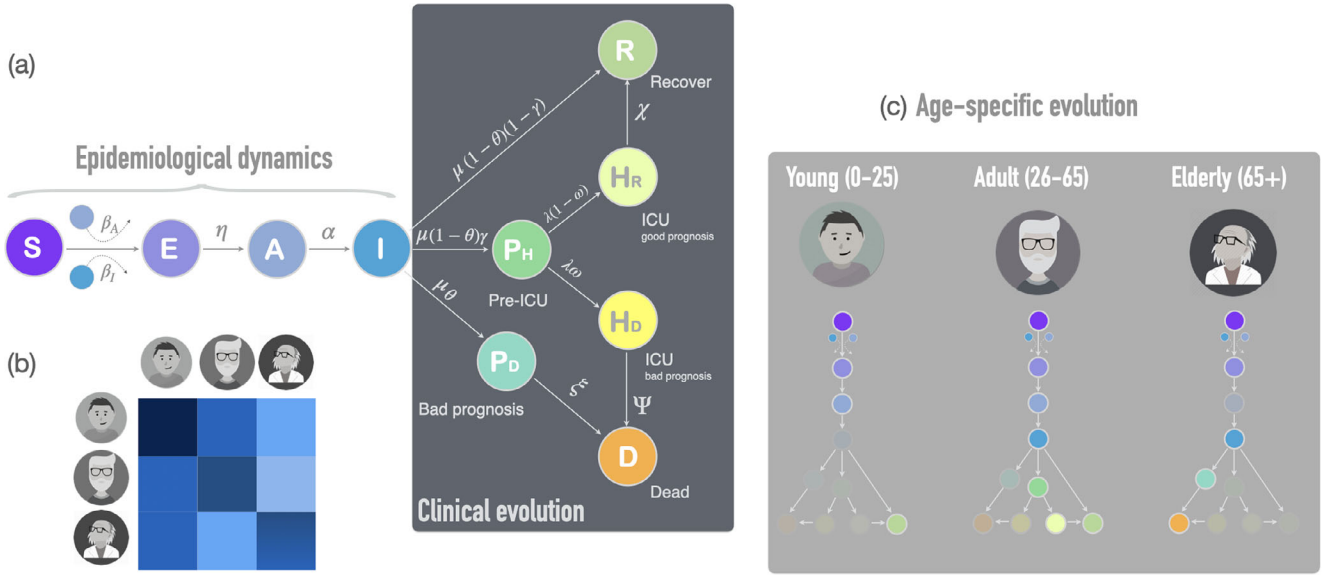

Figure 5. Compartments of the COVID-19 epidemic model. a) We show the compartments and the corresponding transitions between them of the model developed to capture the epidemiological and clinical evolution of COVID-19 cases. The acronyms correspond to: susceptible (S), exposed (E), asymptomatic infectious (A), symptomatic infectious (I), pre-hospitalized in ICU (P_H), pre-deceased (P_D), in ICU before recovery (H_R), in ICU before death (H_D), deceased (D), and recovered (R). The arrows indicate the transition probabilities. The model takes into account three different groups: young (0–25 years old), adults (26–65 years old), and elderly (> 65 years old). In panel (b) we show the connectivity matrix among age groups and in (c) we highlight the most visited compartments for each of the groups, pinpointing that the epidemiological and clinical evolution is age-specific.

targeted quarantine measures, given their critical importance in influencing the pandemic's trajectory. The model facilitates the incorporation of the temporal evolution of the confined population fraction and the evaluation of lockdown policies to curtail the pandemic. Leveraging this feature, the authors examine various epidemic scenarios influenced by distinct containment measures, assessing their effects on reducing epidemic prevalence and alleviating the strain on Spain's healthcare system during March, April, and May 2020. Notably, the model allows for the determination of the minimal confinement level required to prevent a healthcare system collapse while minimizing disruptions to the country's economic structure.

Suppose a population of N individuals distributed in N_p regions, with n_i individuals residing in region (patch) i. Also consider that individuals belong to one of N_G different age strata, in such a way that n_i^g individuals of age strata g live in region i. Thus,

$$N = \sum_{g=1}^{N_G} \sum_{i=1}^{N_P} n_i^g = \sum_{i=1}^{N_P} n_i = \sum_{g=1}^{N_G} n^g \tag{85}$$

where n^g is the total population of age strata g (**Figure 5**).

The system is completely characterized by variables $\rho_i^{m,g}(t)$ which account for the probabilities that individuals of age stratum g assigned to patch i are in state m at time t, where $m \in \{S, E, A, I, P_H, P_D, H_R, H_D, R, D\}$ and $g \in \{Y, M, O\}$. The temporal evolution of these quantities is given by:

$$\rho_i^{S,g}(t+1) = \rho_i^{S,g}(t)\,(1 - \Pi_i^g(t)) \tag{86}$$

$$\rho_i^{E,g}(t+1) = \rho_i^{S,g}(t)\,\Pi_i^g(t) + (1-\eta^g)\,\rho_i^{E,g}(t) \tag{87}$$

$$\rho_i^{A,g}(t+1) = \eta^g\,\rho_i^{E,g}(t) + (1-\alpha^g)\,\rho_i^{A,g}(t) \tag{88}$$

$$\rho_i^{I,g}(t+1) = \alpha^g\,\rho_i^{A,g}(t) + (1-\mu^g)\,\rho_i^{I,g}(t) \tag{89}$$

$$\rho_i^{P_D,g}(t+1) = \mu^g\,\theta^g\,\rho_i^{I,g}(t) + (1-\zeta^g)\,\rho_i^{P_D,g}(t) \tag{90}$$

$$\rho_i^{P_H,g}(t+1) = \mu^g\,(1-\theta^g)\,\gamma^g\,\rho_i^{I,g}(t) + (1-\lambda^g)\,\rho_i^{P_H,g}(t) \tag{91}$$

$$\rho_i^{R,g}(t+1) = \mu^g\,(1-\theta^g)\,(1-\gamma^g)\,\rho_i^{I,g}(t) + \chi^g\,\rho_i^{H_R,g}(t) + \rho_i^{R,g}(t) \tag{92}$$

$$\rho_i^{H_D,g}(t+1) = \lambda^g\,\omega^g\,\rho_i^{P_H,g}(t) + (1-\psi^g)\,\rho_i^{H_D,g}(t) \tag{93}$$

$$\rho_i^{H_R,g}(t+1) = \lambda^g\,(1-\omega^g)\,\rho_i^{P_H,g}(t) + (1-\chi^g)\,\rho_i^{H_R,g}(t) \tag{94}$$

$$\rho_i^{D,g}(t+1) = \zeta^g\,\rho_i^{P_D,g}(t) + \psi^g\,\rho_i^{H_D,g}(t) + \rho_i^{D,g}(t) \tag{95}$$

These MMCA equations correspond to a discrete-time dynamics, in which each time-step represents a day. Note that the sum over all $\rho_i^{m,g}(t)$ for a given patch i and age group g equals 1 for each time step t.

The essence of the described compartmental dynamics centers on the infection process: susceptible individuals become exposed through contact with asymptomatic and symptomatic carriers at a probability $\Pi_i^g(t)$. These exposed individuals may be-

© 2024 The Author(s). Annalen der Physik published by Wiley-VCH GmbH

15213889, 0, Downloaded from https://onlinelibrary.wiley.com/doi/10.1002/andp.202400078 by Universidad De Zaragoza, Wiley Online Library on [12/09/2024]. See the Terms and Conditions (https://onlinelibrary.wiley.com/terms-and-conditions) on Wiley Online Library for rules of use; OA articles are governed by the applicable Creative Commons License

come asymptomatic with probability rate η^g, later becoming infectious at rate α^g. Once infected, three paths emerge, which are reached at an infectious rate μ^g. The first one is death without ICU admission at probability θ^g, after a latency period governed by rate ζ^g. Otherwise, with probability γ^g the individuals are hospitalized in the ICU, which is reached at rate λ^g, while with probability $1-\gamma^g$ they recover. Individuals in the ICU have a fatality probability ω^g, which is reached at a rate ψ^g, whereas the recovery is reached at a rate χ^g.

The study introduces a new way to derive an expression for the effective reproduction number, $\mathcal{R}(t)$, from the MMCA equations that encapsulate both the epidemiological traits of COVID-19 and the social dynamics facilitating its spread. This measure is critical for assessing non-pharmacological interventions' effectiveness, allowing for targeted, minimal-impact strategies.

Focusing on Spain's outbreak, the research evaluates various confinement levels (κ_0) and their effects on epidemic control by examining $\mathcal{R}(t)$ at the start of containment (t_c). This analysis reveals a critical confinement threshold (κ_0^c) distinguishing between a supercritical scenario, where $\mathcal{R}(t_c) > 1$, merely flattening the epidemic curve, and a subcritical scenario, $\mathcal{R}(t_c) < 1$, which significantly alters the social contact structure, effectively hindering viral transmission. This threshold's effectiveness is intricately linked to the specific social structure and mobility patterns inherent to the population. Moreover, its efficacy is contingent upon the timing of its application, reflecting the then-available susceptible population pool that can be effectively isolated. The universality of the $\mathcal{R}(t)$ expression derived from the MMCA facilitates its application across varied populations and can be integrated with any metapopulation epidemic model. This paves the way for the formulation and implementation of timely, evidence-based, and socially considerate non-pharmacological strategies.

7. Conclusion and Perspectives

The Microscopic Markov Chain Approach (MMCA) has been thoroughly examined as a framework for modeling probabilistic spreading processes on networks within a discrete-time context. This methodology is distinguished by its mathematical rigor, computational efficiency, and empirical fidelity, making it a viable tool for practical applications.

Alternative models operating in continuous time are available; however, the derivation of MMCA equations does not invariably stem from the discretization of such continuous dynamics. This distinction arises due to the potential occurrence of multiple concurrent events within a discrete time window, which aligns with the granularity of data availability. This nuance was notably evidenced in the context of COVID-19 forecasting, where the discrete-time MMCA framework provided a critical analytical tool for predicting disease spread, underscoring the importance of adapting model temporal resolution to align with empirical data characteristics.

Within the scope of future research trajectories employing the Microscopic Markov Chain Approach (MMCA) formalism, three prominent avenues emerge. First, the extension of MMCA to encapsulate dynamical processes on hypergraphs presents a significant opportunity. This adaptation would enable the modeling of complex interactions beyond pairwise relationships, thereby capturing the multidimensional interplay characteristic of numerous real-world systems. Although this extension has already started, it is still limited to certain structures and dynamics, thus with a long way to go. Second, the exploration of dynamically evolving spreading processes, wherein both the parameters and the nature of the dynamics themselves exhibit temporal variation, holds considerable promise. An illustrative case pertains to the dissemination and concurrent evolution of ideas, a domain where MMCA could provide profound insights. By integrating the dynamics of idea propagation with the inherent evolution of the ideas themselves, this approach harbors the potential to unravel the intricate mechanisms governing information flow and transformation. Lastly, although the current research in MMCA has predominantly focused on spreading processes, the framework's versatility could be extended to a broader spectrum of applications. For instance, MMCA could be leveraged to model competition dynamics such as evolutionary games, offering a comprehensive understanding of the underlying mechanisms driving these processes.

Collectively, these research directions underscore the versatility and prospective utility of MMCA in addressing sophisticated problems in the realm of network dynamics, promising to illuminate complex phenomena in the next future.

Acknowledgements

A.A., C.G, and S.G. acknowledge support from the Spanish Ministerio de Ciencia e Innovación (PID2021-128005NB-C21), Generalitat de Catalunya (2021SGR-00633), and Universitat Rovira i Virgili (2023PFR-URV-00633), the European Union's Horizon Europe Programme under the CREXDATA project and Program Beatriz Galindo from the Government of Spain.

J.G.G. acknowledges financial support from the Departamento de Industria e Innovación del Gobierno de Aragón y Fondo Social Europeo (FENOL group E-19), grant PID2020-113582GB-I00 funded by MCIN/AEI/10.13039/501100011033, and Fundación Ibercaja and Universidad de Zaragoza (grant 224220).

A.A. acknowledges the Joint Appointment Program at Pacific Northwest National Laboratory (PNNL). PNNL is a multi-program national laboratory operated for the U.S. Department of Energy (DOE) by Battelle Memorial Institute under Contract No. DE-AC05-76RL01830, grant agreement no. 101092749, ICREA Academia, and the James S. McDonnell Foundation (Grant N. 220020325).

Conflict of Interest

The authors declare no conflict of interest.

Keywords

epidemics, modeling, networks

Received: March 14, 2024
Revised: June 24, 2024
Published online:

[1] M. J. Keeling, K. T. Eames, *J. R. Soc., Interface* **2005**, *2*, 295.
[2] M. Newman, *Networks*, Oxford University Press, Oxford New York **2010**.
[3] R. Pastor-Satorras, C. Castellano, P. Van Mieghem, A. Vespignani, *Rev. Mod. Phys.* **2015**, *87*, 925.

© 2024 The Author(s). Annalen der Physik published by Wiley-VCH GmbH

15213889, 0, Downloaded from https://onlinelibrary.wiley.com/doi/10.1002/andp.202400078 by Universidad De Zaragoza, Wiley Online Library on [12/09/2024]. See the Terms and Conditions (https://onlinelibrary.wiley.com/terms-and-conditions) on Wiley Online Library for rules of use; OA articles are governed by the applicable Creative Commons License

[4] I. Z. Kiss, J. C. Miller, P. L. Simon, *Mathematics of Epidemics on Networks: From Exact to Approximate Models*, Springer International Publishing, Berlin **2017**.
[5] L. J. Allen, in *Mathematical Epidemiology*, Springer, Berlin **2008**, pp. 81–130.
[6] S. Bansal, B. T. Grenfell, L. A. Meyers, *J. R. Soc., Interface* **2007**, *4*, 879.
[7] A. L. Lloyd, R. M. May, *J. Theor. Biol.* **1996**, *179*, 1.
[8] T. Gross, C. J. D. D'Lima, B. Blasius, *Phys. Rev. Lett.* **2006**, *96*, 208701.
[9] Z. Wang, C. T. Bauch, S. Bhattacharyya, A. D'Onofrio, P. Manfredi, M. Perc, N. Perra, M. Salathé, D. Zhao, *Phys. Rep.* **2016**, *664*, 1.
[10] C. Granell, S. Gómez, A. Arenas, *Phys. Rev. Lett.* **2013**, *111*, 128701.
[11] L. J. Allen, *Math. Biosci.* **1994**, *124*, 83.
[12] S. Gómez, A. Arenas, J. Borge-Holthoefer, S. Meloni, Y. Moreno, *EPL (Europhys. Lett.)* **2010**, *89*, 38009.
[13] M. Newman, *Networks*, Oxford University Press, Oxford **2018**.
[14] R. Pastor-Satorras, A. Vespignani, *Phys. Rev. E* **2001**, *63*, 066117.
[15] A. L. Lloyd, R. M. May, *Science* **2001**, *292*, 1316.
[16] M. E. J. Newman, *Phys. Rev. E* **2002**, *66*, 016128.
[17] M. Barthélemy, A. Barrat, R. Pastor-Satorras, A. Vespignani, *Phys. Rev. Lett.* **2004**, *92*, 178701.
[18] S. Meloni, A. Arenas, Y. Moreno, *Proc. Natl. Acad. Sci. U.S.A.* **2009**, *106*, 16897.
[19] M. Boguñá, R. Pastor-Satorras, A. Vespignani, *Phys. Rev. Lett.* **2003**, *90*, 028701.
[20] H. W. Hethcote, *Math. Biosci.* **1976**, *28*, 335.
[21] R. Pastor-Satorras, A. Vespignani, *Phys. Rev. Lett.* **2001**, *86*, 3200.
[22] M. Boguñá, C. Castellano, R. Pastor-Satorras, *Phys. Rev. E* **2009**, *79*, 036110.
[23] D. H. Silva, F. A. Rodrigues, S. C. Ferreira, *Phys. Rev. E* **2024**, *110*, 014302.
[24] P. Van Mieghem, J. Omic, R. Kooij, *IEEE/ACM Trans. Netw.* **2008**, *17*, 1.
[25] P. L. Simon, M. Taylor, I. Z. Kiss, *J. Math. Biol.* **2011**, *62*, 479.
[26] P. Van Mieghem, E. Cator, *Phys. Rev. E* **2012**, *86*, 016116.
[27] H. W. Hethcote, *SIAM Rev.* **2000**, *42*, 599.
[28] D. Chakrabarti, Y. Wang, C. Wang, J. Leskovec, C. Faloutsos, *ACM Trans. Inform. Syst. Sec.* **2008**, *10*, 4.
[29] S. Gómez, J. Gómez-Gardeñes, Y. Moreno, A. Arenas, *Phys. Rev. E* **2011**, *84*, 036105.
[30] A. Arenas, A. Garijo, S. Gómez, J. Villadelprat, *Chaos, Solitons Fractals* **2023**, *166*, 112921.
[31] J. T. Matamalas, A. Arenas, S. Gómez, *Sci. Adv.* **2018**, *4*, eaau4212.
[32] M. Granovetter, *Am. J. Sociol.* **1978**, *83*, 1420.
[33] D. J. Watts, *Proc. Natl. Acad. Sci. U.S.A.* **2002**, *99*, 5766.
[34] P. S. Dodds, D. J. Watts, *Phys. Rev. Lett.* **2004**, *92*, 218701.
[35] D. Centola, M. Macy, *Am. J. Sociol.* **2007**, *113*, 702.
[36] D. Guilbeault, J. Becker, D. Centola, in *Complex Spreading Phenomena in Social Systems: Influence and Contagion in Real-World Social Networks*, Springer International Publishing, Cham **2018**, pp. 3–25.
[37] P. Romanczuk, B. C. Daniels, in *Order, Disorder and Criticality: Advanced Problems of Phase Transition Theory*, World Scientific, Singapore **2023**, pp. 179–208.
[38] W. Goffman, V. Newill, *Nature* **1964**, *204*, 225.
[39] D. J. Daley, D. G. Kendall, *Nature* **1964**, *204*, 1118.
[40] D. A. Levy, P. R. Nail, *Gen. Soc. Gen. Psychol. Monogr.* **1993**, *119*, 233.
[41] A. L. Hill, D. G. Rand, M. A. Nowak, N. A. Christakis, *PLOS Comput. Biol.* **2010**, *6*, 1000968.
[42] G. Burgio, A. Arenas, S. Gómez, J. T. Matamalas, *Commun. Phys.* **2021**, *4*, 111.
[43] The number of maximal edges, regardless of cardinality, must increase at a rate slower than quadratic relative to the system size.
[44] Note that this closure achieves exactness for non-recursive dynamics, such as the susceptible-infected-recovered (SIR) processes, in structures devoid of cycles exceeding three nodes.[4]
[45] G. Burgio, S. Gómez, A. Arenas, *Phys. Rev. Lett.* **2024**, *132*, 077401.
[46] Notice that the permutation of the superscripts σ, σ', and σ has no effect.
[47] J. T. Matamalas, S. Gómez, A. Arenas, *Phys. Rev. Res.* **2020**, *2*, 012049.
[48] E. Valdano, L. Ferreri, C. Poletto, V. Colizza, *Phys. Rev. X* **2015**, *5*, 021005.
[49] M. De Domenico, A. Solé-Ribalta, E. Cozzo, M. Kivelä, Y. Moreno, M. A. Porter, S. Gómez, A. Arenas, *Phys. Rev. X* **2013**, *3*, 041022.
[50] E. Cozzo, R. A. Baños, S. Meloni, Y. Moreno, *Phys. Rev. E* **2013**, *88*, 050801.
[51] Y. Wang, D. Chakrabarti, C. Wang, C. Faloutsos, in *22nd Int. Symp. Reliable Distrib. Syst. 2003. Proc.* IEEE, **2003**, pp. 25–34.
[52] M. Kivelä, A. Arenas, M. Barthelemy, J. P. Gleeson, Y. Moreno, M. A. Porter, *J. Complex Netw.* **2014**, *2*, 203.
[53] S. Boccaletti, G. Bianconi, R. Criado, C. I. Del Genio, J. Gómez-Gardenes, M. Romance, I. Sendina-Nadal, Z. Wang, M. Zanin, *Phys. Rep.* **2014**, *544*, 1.
[54] M. Dickison, S. Havlin, H. E. Stanley, *Phys. Rev. E* **2012**, *85*, 066109.
[55] J. Sanz, C.-Y. Xia, S. Meloni, Y. Moreno, *Phys. Rev. X* **2014**, *4*, 041005.
[56] M. Salehi, R. Sharma, M. Marzolla, M. Magnani, P. Siyari, D. Montesi, *IEEE Trans. Netw. Sci. Eng.* **2015**, *2*, 65.
[57] G. F. de Arruda, E. Cozzo, T. P. Peixoto, F. A. Rodrigues, Y. Moreno, *Phys. Rev. X* **2017**, *7*, 011014.
[58] Z. Wang, M. A. Andrews, L. Wang, C. T. Bauch, *Phys. Life Rev.* **2015**, *15*, 1.
[59] S. Funk, S. Bansal, C. T. Bauch, K. T. Eames, W. J. Edmunds, A. P. Galvani, P. Klepac, *Epidemics* **2015**, *10*, 21.
[60] S. Funk, E. Gilad, C. Watkins, V. A. A. Jansen, *Proc. Natl. Acad. Sci. U.S.A.* **2009**, *106*, 6872.
[61] C. Granell, S. Gómez, A. Arenas, *Phys. Rev. E* **2014**, *90*, 012808.
[62] A. Saumell-Mendiola, M. A. Serrano, M. Boguñá, *Phys. Rev. E* **2012**, *86*, 026106.
[63] G. Ferraz de Arruda, F. Aparecido Rodrigues, P. Martín Rodríguez, E. Cozzo, Y. Moreno, *J. Complex Netw.* **2017**, *6*, 215.
[64] S. Funk, V. A. A. Jansen, *Phys. Rev. E* **2010**, *81*, 036118.
[65] Y. Nie, W. Li, L. Pan, T. Lin, W. Wang, *Appl. Math. Comput.* **2022**, *417*, 126773.
[66] J. Chen, Y. Liu, M. Tang, J. Yue, *Inf. Sci.* **2023**, *619*, 478.
[67] D. Soriano-Paños, F. Ghanbarnejad, S. Meloni, J. Gómez-Gardeñes, *Phys. Rev. E* **2019**, *100*, 062308.
[68] F. Ball, T. Britton, T. House, V. Isham, D. Mollison, L. Pellis, G. S. Tomba, *Epidemics* **2015**, *10*, 63.
[69] M. C. González, C. A. Hidalgo, A.-L. Barabási, *Nature* **2008**, *453*, 779.
[70] H. Barbosa, M. Barthelemy, G. Ghoshal, C. R. James, M. Lenormand, T. Louail, R. Menezes, J. J. Ramasco, F. Simini, M. Tomasini, *Phys. Rep.* **2018**, *734*, 1.
[71] V. Colizza, R. Pastor-Satorras, A. Vespignani, *Nat. Phys.* **2007**, *3*, 276.
[72] V. Colizza, A. Vespignani, *Phys. Rev. Lett.* **2007**, *99*, 148701.
[73] V. Colizza, A. Vespignani, *J. Theor. Biol.* **2008**, *251*, 450.
[74] D. Balcan, V. Colizza, B. Gonçalves, H. Hu, J. J. Ramasco, A. Vespignani, *Proc. Natl. Acad. Sci. U.S.A* **2009**, *106*, 21484.
[75] D. Balcan, A. Vespignani, *Nat. Phys.* **2011**, *7*, 581.
[76] V. Belik, T. Geisel, D. Brockmann, *Phys. Rev. X* **2011**, *1*, 011001.
[77] D. Balcan, A. Vespignani, *J. Theor. Biol.* **2012**, *293*, 87.
[78] V. Belik, T. Geisel, D. Brockmann, *Europ. Phys. J. B* **2011**, *84*, 579.
[79] S. Charaudeau, K. Pakdaman, P.-Y. Boëlle, *PLoS One* **2014**, *9*, 83002.
[80] A. Apolloni, C. Poletto, J. J. Ramasco, P. Jensen, V. Colizza, *Sci. Rep.* **2014**, *4*, 4857.
[81] P. Bosetti, P. Poletti, M. Stella, B. Lepri, S. Merler, M. De Domenico, *Proc. Natl. Acad. Sci. U.S.A.* **2020**, *117*, 30118.

© 2024 The Author(s). Annalen der Physik published by Wiley-VCH GmbH

15213889, 0, Downloaded from https://onlinelibrary.wiley.com/doi/10.1002/andp.202400078 by Universidad De Zaragoza, Wiley Online Library on [12/09/2024]. See the Terms and Conditions (https://onlinelibrary.wiley.com/terms-and-conditions) on Wiley Online Library for rules of use; OA articles are governed by the applicable Creative Commons License

[82] P. Castioni, R. Gallotti, M. De Domenico, *Commun. Phys.* **2021**, *4*, 131.
[83] M. Mazzoli, R. Gallotti, F. Privitera, P. Colet, J. Ramasco, *Nat. Commun.* **2023**, *14*, 1448.
[84] D. Soriano-Paños, W. Cota, S. C. Ferreira, G. Ghoshal, A. Arenas, J. Gómez-Gardeñes, *Ann. Phys.* **2022**, *534*, 2100482.
[85] J. Gómez-Gardeñes, D. Soriano-Paños, A. Arenas, *Nat. Phys.* **2018**, *14*, 391.
[86] C. Granell, P. J. Mucha, *Phys. Rev. E* **2018**, *97*, 5.
[87] S. V. Scarpino, *Nat. Phys.* **2018**, *14*, 331.
[88] D. Soriano-Paños, L. Lotero, A. Arenas, J. Gómez-Gardeñes, *Phys. Rev. X* **2018**, *8*, 031039.
[89] D. Soriano-Paños, G. Ghoshal, A. Arenas, J. Gómez-Gardeñes, *J. Stat. Mech.: Theory Exp.* **2020**, *2020*, 024006.
[90] W. Cota, D. Soriano-Paños, A. Arenas, S. C. Costa, J. Gómez-Gardeñes, *New J. Phys.* **2021**, *23*, 073019.
[91] P. Valgañón, D. Soriano-Paños, A. Arenas, J. Gómez-Gardeñes, *Chaos: Interdisciplin. J. Nonlinear Sci.* **2022**, *32*, 043102.
[92] A. Arenas, W. Cota, J. Gómez-Gardeñes, S. Gómez, C. Granell, J. T. Matamalas, D. Soriano-Paños, B. Steinegger, *Phys. Rev. X* **2020**, *10*, 041055.
[93] G. S. Costa, W. Cota, S. C. Ferreira, *Phys. Rev. Res.* **2020**, *2*, 043306.
[94] S. Hazarie, D. Soriano-Paños, A. Arenas, J. Gómez-Gardeñes, G. Ghoshal, *Commun. Phys.* **2021**, *4*, 1.
[95] D. Soriano-Paños, J. H. Arias-Castro, A. Reyna-Lara, H. J. Martínez, S. Meloni, J. Gómez-Gardeñes, *Phys. Rev. Res.* **2020**, *2*, 013312.
[96] C. Ospina-Aguirre, D. Soriano-Paños, G. Olivar-Tost, C. C. Galindo-González, J. Gómez-Gardeñes, G. Osorio, *PLoS Neglected Trop. Dis.* **2023**, *17*, 1.
[97] X. Zhu, Y. Liu, S. Wang, R. Wang, X. Chen, W. Wang, *Appl. Math. Comput.* **2021**, *411*, 126531.
[98] A. Reyna-Lara, D. Soriano-Paños, J. H. Arias-Castro, H. J. Martínez, J. Gómez-Gardeñes, *Chaos: Interdisciplin. J. Nonlinear Sci.* **2022**, *32*, 041105.
[99] B. Wang, M. Gou, Y. Han, *Nonlinear Dyn.* **2021**, *105*, 3835.
[100] A. Reyna-Lara, D. Soriano-Paños, A. Arenas, J. Gómez-Gardeñes, *Chaos, Solitons Fractals* **2022**, *158*, 112012.
[101] CDC, COVID-19 Pandemic Planning Scenarios. CDC (USA), Technical report, Centers for Disease Control and Prevention, **2020**, https://www.cdc.gov/coronavirus/2019-ncov/hcp/planning-scenarios.html (accessed: August 2020).
[102] J. T. Wu, K. Leung, G. M. Leung, *Lancet* **2020**, *395*, 689.
[103] S. Bialek, E. Boundy, V. Bowen, N. Chow, A. Cohn, N. Dowling, S. Ellington, R. Gierke, A. Hall, J. MacNeil, P. Patel, G. Peacock, T. Pilishvili, H. Razzaghi, N. Reed, M. Ritchie, E. Sauber-Schatz, *MMWR. Morb. Mort. Weekly Rep.* **2020**, *69*, 12.
[104] F. Zhou, T. Yu, R. Du, G. Fan, Y. Liu, Z. Liu, J. Xiang, Y. Wang, B. Song, X. Gu, L. Guan, Y. Wei, H. Li, X. Wu, J. Xu, S. Tu, Y. Zhang, H. Chen, B. Cao, *Lancet* **2020**, *395*, 1054.
[105] Q. Bi, Y. Wu, S. Mei, C. Ye, X. Zou, Z. Zhang, X. Liu, L. Wei, S. A. Truelove, T. Zhang, W. Gao, C. Cheng, X. Tang, X. Wu, Y. Wu, B. Sun, S. Huang, Y. Sun, J. Zhang, T. Ma, J. Lessler, T. Feng, *Lancet Infect. Dis.* **2020**, *20*, 911.

Clara Granell Clara Granell is Associate Professor at Universitat Rovira i Virgili. Her work mainly focuses on the study of Complex Systems, mainly developing models for epidemic spreading, but also neuronal networks and community detection on Complex Networks.

Sergio Gómez Sergio Gómez is Associate Professor at Universitat Rovira i Virgili. His works focus on the study of the structure of complex networks and dynamics on top of them, using physical, mathematical, and computational approaches.

© 2024 The Author(s). Annalen der Physik published by Wiley-VCH GmbH

15213889, 0, Downloaded from https://onlinelibrary.wiley.com/doi/10.1002/andp.202400078 by Universidad De Zaragoza, Wiley Online Library on [12/09/2024]. See the Terms and Conditions (https://onlinelibrary.wiley.com/terms-and-conditions) on Wiley Online Library for rules of use; OA articles are governed by the applicable Creative Commons License

Jesús Gómez-Gardeñes Jesús Gómez-Gardeñes is a full Professor at the University of Zaragoza where he leads the group of theoretical and applied modeling of the Institute for Biocomputation and Physics of Complex Systems. His works focus on applying statistical physics and nonlinear dynamics approaches to shed light on the basic mechanisms and interactions that shape the collective behavior of real-world complex systems.

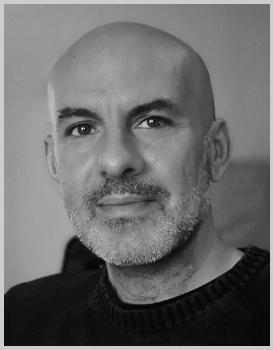

Alex Arenas Alex Arenas is a full Professor at Universitat Rovira i Virgili. In 2019, he was elected as Fellow of the American Physical Society, in 2020, he was elected as Fellow of the Network Science Society, and in 2021 he received the award—Narcis Monturiol Medal. His works focus on applying statistical physics and nonlinear dynamics to real-world complex systems, with special interest in the physics of epidemics, synchronization and urban systems.

© 2024 The Author(s). Annalen der Physik published by Wiley-VCH GmbH

15213889, 0, Downloaded from https://onlinelibrary.wiley.com/doi/10.1002/andp.202400078 by Universidad De Zaragoza, Wiley Online Library on [12/09/2024]. See the Terms and Conditions (https://onlinelibrary.wiley.com/terms-and-conditions) on Wiley Online Library for rules of use; OA articles are governed by the applicable Creative Commons License